

1 **A simple object-oriented and open source model for scientific and policy analyses of**
2 **the global climate system–Hector v1.0**

3 C.A. Hartin*, P. Patel, A. Schwarber, R.P. Link, and B.P. Bond-Lamberty

4

5 Pacific Northwest National Laboratory, Joint Global Change Research Institute at the
6 University of Maryland–College Park, 5825 University Research Court, College Park, MD
7 20740, USA

8

9 *Corresponding author: corinne.hartin@pnnl.gov

10

11

12 **Abstract**

13 Simple climate models play an integral role in the policy and scientific communities.
14 They are used for climate mitigation scenarios within integrated assessment models,
15 complex climate model emulation, and uncertainty analyses. Here we describe Hector
16 v1.0, an open source, object-oriented, simple global climate carbon-cycle model. This
17 model runs essentially instantaneously while still representing the most critical global
18 scale earth system processes. Hector has a three-part main carbon cycle: a one-pool
19 atmosphere, land, and ocean. The model's terrestrial carbon cycle includes primary
20 production and respiration fluxes, accommodating arbitrary geographic divisions into,
21 e.g., ecological biomes or political units. Hector actively solves the inorganic carbon
22 system in the surface ocean, directly calculating air-sea fluxes of carbon and ocean pH.
23 Hector reproduces the global historical trends of atmospheric [CO₂], radiative forcing,
24 and surface temperatures. The model simulates all four Representative Concentration
25 Pathways with equivalent rates of change of key variables over time compared to
26 current observations, MAGICC (a well-known simple climate model), and models from
27 the 5th Coupled Model Intercomparison Project. Hector's flexibility, open source nature,
28 and modular design will facilitate a broad range of research in various areas.

29

30

31 **1.0 Introduction**

32 Projecting future impacts of anthropogenic perturbations on the climate system
33 relies on understanding the interactions of key earth system processes. To accomplish
34 this, a hierarchy of climate models with differing levels of complexity and resolution are
35 used, ranging from purely statistical or empirical models, to simple energy balance
36 models, to fully-coupled Earth System Models (ESMs) (Stocker, 2011).

37 Reduced-complexity or simple climate models (SCMs) lie in the middle of this
38 spectrum, representing only the most critical global scale earth system processes with
39 low spatial and temporal resolution, e.g., carbon fluxes between the ocean and
40 atmosphere, primary production and respiration fluxes on land. These models are
41 relatively easy to use and understand, and are computationally inexpensive. Most SCMs
42 have a few key features: 1) calculating future concentrations of greenhouse gases
43 (GHGs) from given emissions while modeling the global carbon cycle; 2) calculating
44 global mean radiative forcing from greenhouse gas concentrations; and 3) converting
45 the radiative forcing to global mean temperature (e.g., Wigley, 1991; Meinshausen et al.,
46 2011a; Tanaka et al., 2007b; Lenton, 2000).

47 With these capabilities, SCMs play an integral role in decision making and scientific
48 research. For example, energy-economic-climate models or Integrated Assessment
49 Models (IAMs) are used to address issues on energy system planning, climate mitigation,
50 stabilization pathways, and land-use changes (Wigley et al., 1996; Edmonds and Smith,
51 2006; van Vuuren et al., 2011). ESMs are too computationally expensive to use in these

52 analyses. Therefore, all IAMs rely on a simple representation of the global climate
53 system.

54 Depending on the purpose of the IAMs (economics, cost-benefit analysis, or more
55 physical based processes), the corresponding climate and carbon component varies in
56 complexity and resolution. For example, models like DICE, FUND, and MERGE have a
57 highly simplified carbon/climate system (Nordhaus, 2008; Anthoff and Tol, 2014; Manne
58 and Richels, 2005). IAMs focusing more on the physical processes of the natural system
59 and the economy employ more complex representations of the climate/carbon system.
60 Models like GCAM (Global Change Assessment Model) and MESSAGE use MAGICC as
61 their SCM (Meinshausen et al., 2011a; Riahi et al., 2007; Calvin et al., 2011). Increasing
62 in complexity, some IAMs include the climate/carbon system at gridded scales (e.g.,
63 IMAGE), and can be coupled to earth system models of intermediate complexity (e.g.,
64 MIT IGSM), or more recently coupled to a full earth system model (the iESM project)
65 (Bouwman et al., 2006; Sokolov et al., 2005; Bond-Lamberty et al., 2014; Di Vittorio et
66 al., 2014; Collins et al., 2015).

67 SCMs such as MAGICC, GENIE, and the climate emulation tool at RDCEP are also
68 used as emulators of more complex ESMs (Meinshausen et al., 2011c; Schlesinger and
69 Jiang, 1990; Challenor, 2012; Ratto et al., 2012; Lenton et al., 2009; Castruccio et al.,
70 2014). The behavior of SCMs can be constrained to replicate the overall behavior of the
71 more complex ESM. For instance, the climate sensitivity of a SCM can be made equal to
72 that of an ESM by altering a single model parameter. In particular, the MAGICC model
73 has been central to the analyses presented in the Intergovernmental Panel on Climate

74 Change (IPCC) reports, and can be parameterized to emulate a large suite of ESMs
75 (Meinshausen et al., 2011a).

76 Lastly, SCMs are computationally efficient and inexpensive to run. Therefore, they
77 are used to run multiple simulations of future climate change emissions scenarios,
78 parameter sensitivity experiments, perturbed physics experiments, large ensemble runs,
79 and uncertainty analyses (Senior and Mitchell, 2000; Hoffert et al., 1980; Harvey and
80 Schneider, 1985; Ricciuto et al., 2008; Sriver et al., 2012; Irvine et al., 2012). MAGICC,
81 the Bern CC model, and SNEASY are examples of a few models used for uncertainty
82 analysis (Meinshausen et al., 2011c; Urban and Keller, 2010; Joos et al., 2001b). SCMs
83 have been useful in reducing uncertainties in future CO₂ sinks, quantifying parametric
84 uncertainties in sea-level rise, ice-sheet modeling, ocean-heat uptake, and aerosol
85 forcing (Ricciuto et al., 2008; Sriver et al., 2012; Applegate et al., 2012; Urban and Keller,
86 2009).

87 This study introduces Hector v1.0, an open source, object-oriented, simple climate
88 carbon-cycle model. Hector was developed with three main goals in mind. First, Hector
89 is an open source model, an important quality given that the scientific community,
90 funding agencies, and journals are increasingly emphasizing transparency and open
91 source (E.P. White, 2013; Heron et al., 2013), particularly in climate change sciences
92 (Wolkovich et al., 2012). A large community of scientists can access, use, and enhance
93 open source models, with the potential for long-term utilization, improvement, and
94 reproducibility (Ince et al., 2012). Second, a clean design using an object-oriented
95 framework is critical for Hector development and future use. This allows for new

96 components to easily be added to Hector, i.e. the model's functionality to be easily
97 extended in the future. In addition, this framework allows for easy coupling into IAMs,
98 in particular GCAM. Lastly, Hector is a stand-alone simple climate model used to answer
99 fundamental scientific research questions, uncertainty analysis, parameter sensitivities,
100 etc.

101 One of the fundamental questions faced in developing a SCM is how much detail
102 should be represented in the climate system. Our goal is to introduce complexity only
103 where warranted, keeping the representations of the climate system as simple as
104 possible. This results in fewer calculations, faster execution times, and easier analysis
105 and interpretation of results. Sections 2, 3, and 4 describe the structure and
106 components of Hector. Sections 5 and 6 describe the experiments, results and
107 comparison of Hector against observational data and other models (MAGICC and
108 CMIP5).

109

110 **2.0 Model architecture**

111 **2.1 Overall structure and design**

112 Hector is written in C++ and uses an object-oriented design that enforces clean
113 separation between its different parts, which interact via strictly defined interfaces. The
114 separation keeps each software module self-contained, which makes the code easy for
115 users to understand, maintain, and enhance. Entities in the model include a command-
116 line *wrapper*, the model *coupler*, various *components* organized around scientific areas

117 (carbon cycling, radiative forcing, etc.) and *visitors* responsible for model output. Each of
118 these is discussed below.

119 **2.2 Model Coupler**

120 Hector's control flow starts with the coupler, which is responsible for: 1) parsing
121 and routing input data to the model components; 2) tracking how the components
122 depend on each other; 3) passing messages and data between components; 4) providing
123 facilities for logging, time series interpolation, etc.; and 5) controlling the main model
124 loop as it progresses through time. Any errors thrown by the model are caught by the
125 wrapper, which prints a detailed summary of the error.

126 Input data are specified in flat text files, and during startup are routed to the
127 correct model component for its initialization. Some of the key initial model conditions
128 are summarized in **Table 1 and Table 2**. For more details of initial model conditions we
129 urge the reader to download Hector v1.0 (<https://github.com/JGCRI/hector>).

130 Components can send messages to each other during the model run, most often
131 requesting data. The messaging interface is also available to external subroutines, such
132 as components of IAMs or other linked models. The coupler handles message routing
133 (via the *capability* mechanism, below) and enforces mandatory type checking: e.g., if a
134 component requests mean global temperature in °C but the data are provided in K, an
135 error will be thrown (i.e., execution halts) unless the receiving component can handle
136 this situation.

137 Visitor patterns are units of code that traverse all model components and handle
138 model output (Martin et al., 1997). Two visitors currently exist: one saves an easily-

139 readable summary table to an output file, while the other writes a stream of model data
140 (both standard outputs and internal diagnostics). After the model finishes, this ‘stream’
141 file can be parsed and summarized by R scripts (R Development Core Team, 2014)
142 included with Hector. Log files may also be written by any model entity, using facilities
143 provided by the coupler. The full sequence of events during a model run is summarized
144 in **Figure 1**.

145 **2.3 Components**

146 Model components are submodels that communicate with the coupler. From
147 the coupler’s point of view, components are fully defined by their *capabilities* and
148 *dependencies*. At model startup, before the run begins, components inform the coupler
149 of their capabilities, i.e., what data they can provide to or accept from the larger model
150 system. The coupler uses this information to route messages, such as requests for data,
151 between components. Components also register their dependencies, i.e., what results
152 they require from other components in order to complete their computations. After
153 initialization, but before the model begins to run, the coupler uses this dependency
154 information to determine the order in which components will be called in the main
155 control loop.

156 The model’s modular architecture, and the *capability/dependency* systems
157 described above, allows swapping, enabling and disabling of model components directly
158 via the input without recompiling. For example, this means that a user can test two
159 different ocean submodels and easily compare results without having to rebuild the
160 model.

161 **2.4 Time step, spinup, and constraints**

162 The model's fundamental time step is 1 year, although the carbon cycle can
163 operate on a finer resolution when necessary (Section 3.1). When the model is on an
164 integer date (e.g. 1997.0) it is considered to be the midpoint of that particular calendar
165 year, in accordance with Representative Concentration Pathway (RCP) data
166 (Meinshausen et al., 2011b).

167 Like many models, Hector has an optional 'spinup' step, in which the model runs
168 to equilibrium in an a historical, perturbation-free mode (Pietsch and Hasenauer, 2006).
169 This occurs after model initialization, but before the historical run begins, and ensures
170 that the model is in steady state when it enters the main simulation. During spinup, the
171 coupler repeatedly calls all the model components in their dependency-driven ordering,
172 using an annual time step. Each component signals whether it needs further steps to
173 stabilize, and this process repeats until all components signal that they are complete.

174 Currently only the model's carbon cycle makes use of the spinup phase. Spinup
175 takes place prior to land use change or industrial emission inputs, and the main carbon
176 cycle moves from its initial, user-defined carbon pool values to a steady state in which
177 $dC/dt < \epsilon$ for all pools. The convergence criterion ϵ is user-definable; by default $\epsilon = 1 \text{ Tg}$
178 C yr^{-1} . From its default values the preindustrial carbon cycle will typically stabilize in 300-
179 400 time steps.

180 Hector can be forced to match its output to a user-supplied time series. This is
181 helpful to isolate and test different components. Available constraints currently include
182 atmospheric CO_2 , global temperature anomaly, total ocean-atmosphere carbon

183 exchange, total land-atmosphere carbon exchange, and total radiative forcing. Most
184 constraints operate by overwriting model-calculated values with user-supplied time
185 series data during the run. The atmospheric [CO₂] constraint operates slightly
186 differently, as the global carbon cycle is subject to a continuous mass-balance check. As
187 a result, when the user supplies a [CO₂] record between arbitrary dates and orders the
188 model to match it, the model *computes* [CO₂] at each time step, and any deficit (surplus)
189 in comparison with the constraint [CO₂] is drawn from (added to) the deep ocean. The
190 deep ocean holds the largest reservoir of carbon; therefore, small changes in this large
191 pool have a negligible effect on the carbon cycle dynamics. When the model exits the
192 constraint time period, atmospheric [CO₂] again becomes fully prognostic.

193 **2.5 Code availability and dependencies**

194 All Hector code is open source and available at
195 <https://github.com/JGCRI/hector/>. The repository includes model code that can be
196 compiled on Mac, Linux, and Windows, input files for the four Representative
197 Concentration Pathways (RCP) cases discussed in Section 5, R scripts to process model
198 output, and extensive documentation. Software dependencies are as limited as possible,
199 with only the GNU Scientific Library (GSL, Gough, 2009) and the Boost C++ libraries
200 (<http://www.boost.org>) required. HTML documentation can be automatically generated
201 from the code using the Doxygen tool (<http://www.doxygen.org>). All these tools and
202 libraries are free and open source.

203 In keeping with Hector's emphasis on modern, robust software design, the code
204 includes an optional (i.e., not needed to compile and run the model) unit testing build

205 target. Unit testing allows individual units of source code to be tested in a standardized
206 and automatic manner, ensuring that they behave as expected after changes are made
207 to the model source code. Current tests verify the behavior of the model coupler
208 (message passing and dependency calculation); reading of input; time series; logging;
209 and units checking. This functionality requires the 'googletest' library
210 (<http://code.google.com/p/googletest>).

211

212 **3.0 Carbon Cycle**

213 In the model's default terrestrial carbon cycle, terrestrial vegetation, detritus,
214 and soil are linked with each other and the atmosphere by first-order differential
215 equations (**Figure 2**). Vegetation net primary production is a function of atmospheric
216 [CO₂] and temperature. Carbon flows from the vegetation to detritus and then to soil,
217 losing fractions to heterotrophic respiration on the way. Land-use change emissions are
218 specified as inputs. An 'earth' pool debits carbon emitted as anthropogenic emissions,
219 allowing a continual mass-balance check across the entire carbon cycle.

220 More formally, any change in atmospheric carbon, and thus [CO₂], occurs as a
221 function of anthropogenic fossil fuel and industrial emissions (F_A), land-use change
222 emissions (F_{LC}), and the atmosphere-ocean (F_O) and atmosphere-land (F_L) carbon fluxes.
223 The atmosphere is treated as a single well-mixed box whose rate of change is:

$$\frac{dC_{atm}}{dt} = F_A(t) + F_{LC}(t) - F_O(t) - F_L(t) \quad (1)$$

224 Note that the carbon cycle is solved under indeterminate time steps
225 (represented in the text by equations with d/dt), while most other submodels of Hector

226 are solved under a fixed time step of 1 year (equations with Δ). Future versions of
 227 Hector will incorporate indeterminate time steps within all components of the model.
 228 The overall terrestrial carbon balance (Equation 2) excluding user-specified land-use
 229 change fluxes at time t is the difference between net primary production (NPP) and
 230 heterotrophic respiration (RH). This is summed over user-specified n groups (each
 231 typically regarded as a latitude band, biome, or political unit), with $n \geq 1$:

$$F_L(t) = \sum_{i=1}^n NPP_i(t) - RH_i(t) \quad (2)$$

232 Note that NPP here is assumed to include non-LUC disturbance effects (e.g., fire), for
 233 which there is currently no separate term. For each biome i , NPP is computed as a
 234 function of its preindustrial values NPP_0 , current atmospheric carbon C_{atm} , and the
 235 biome's temperature anomaly T_i , while heterotrophic respiration RH depends upon the
 236 pool sizes of detritus (C_d) and soil (C_s), and global temperatures:

$$NPP_i(t) = NPP_0 * f(C_{atm}, \beta_i) \quad (3)$$

$$f(C_{atm}, \beta_i) = 1 + \beta_i \left(\log \left(\frac{C_{atm}}{C_0} \right) \right) \quad (4)$$

$$RH_{s,d}(t) = C_{s,d} * f_{rs,rd} * Q_{10}^{T_i(t)/10} \quad (5)$$

$$T_i(t) = T_G(t) * \delta_i \quad (6)$$

237 These are commonly used formulations: NPP is modified by a user-specified
 238 carbon fertilization parameter, β (Piao et al., 2013), that is constant in time but not
 239 necessarily in space. For example, users can define separate β values for different
 240 biomes. RH changes are controlled by a biome-specific Q_{10} value. Biomes can
 241 experience temperature changes at rates that differ from the global mean T_G , controlled

242 by a user specified temperature factor δ_i . Note that in equation (5), soil RH depends on a
 243 running mean of past temperatures, representing the slower propagation of heat
 244 through soil strata. Land carbon pools (vegetation, detritus, and soil) change as a result
 245 of NPP , RH , and land-use change fluxes, whose effects are partitioned among these
 246 carbon pools. In addition, carbon flows from vegetation to detritus and to soil (**Figure 2**).
 247 Partitioning fractions (f) control the flux quantities between pools (**Table 2**). For
 248 simplicity Equations 7-9 omit the time t and biome-specific i notations, but each pool is
 249 tracked separately for each biome at each time step:

$$\frac{dC_V}{dt} = NPP f_{nv} - C_V(f_{vd} + f_{vs}) - F_{LC} f_{lv} \quad (7)$$

$$\frac{dC_D}{dt} = NPP f_{nd} + C_V f_{vd} - C_D f_{ds} - RH_{det} - F_{LC} f_{ld} \quad (8)$$

$$\frac{dC_S}{dt} = NPP f_{ns} + C_V f_{vs} + C_D f_{ds} - RH_{soil} - F_{LC} f_{ls} \quad (9)$$

250 The ocean-atmosphere carbon flux is the sum of the ocean's surface fluxes (F_i)
 251 (currently $n=2$, high and low latitude surface box):

$$F_O(t) = \sum_{i=1}^n F_i(t) \quad (10)$$

252 The surface fluxes of each individual box are directly calculated from an ocean chemistry
 253 submodel described in detail by Hartin et al. (in prep). We model the nonlinearity of the
 254 inorganic carbon cycle, calculating pCO_2 , pH, and carbonate saturations based on
 255 equations from Zeebe and Wolf-Gladrow, (2001). The flux of CO_2 for each box i is
 256 calculated by:

$$F_i(t) = k \alpha \Delta pCO_2 \quad (11)$$

257 where k is the CO₂ gas-transfer velocity, α is the solubility of CO₂ in water based on
 258 salinity, temperature, and pressure, and $\Delta p\text{CO}_2$ is the atmosphere-ocean gradient of
 259 pCO₂ (Takahashi et al., 2009). The calculation of pCO₂ in each surface box is based on
 260 the concentration of CO₂ in the ocean and its solubility (a function of temperature,
 261 salinity, and pressure). At steady state, the cold high latitude surface box (>55°, subpolar
 262 gyres) acts as a sink of carbon from the atmosphere, while the warm low latitude
 263 surface box (<55°) off gases carbon back to the atmosphere. Temperatures of the
 264 surface boxes are linearly related to atmospheric global temperatures (see section 4.1),
 265 $T_{\text{HL}} = \Delta T - 13$ and $T_{\text{LL}} = \Delta T + 7$ (Lenton, 2000). The ocean model, modeled after Lenton et
 266 al. (2000) and Knox and McElroy (1984), circulates carbon through four boxes (two
 267 surface, one intermediate depth, one deep), via water mass advection and exchange,
 268 simulating a simple thermohaline circulation (**Figure 2**). At steady state, approximately
 269 100Pg of carbon are transferred from the high latitude surface box to the deep box
 270 based on the volume of the box and transport in Sv ($10^6 \text{ m}^3 \text{ s}^{-1}$) between the boxes. The
 271 change in carbon of any box i is given by the fluxes in and out, with $F_{\text{atm} \rightarrow i}$ as the
 272 atmosphere-ocean carbon flux:

$$\frac{dC_i}{dt} = \sum_{j=1}^{in} F_{j \rightarrow i} - \sum_{j=1}^{out} F_{i \rightarrow j} + F_{\text{atm} \rightarrow i} \quad (12)$$

273 As the model advances, the carbon in PgC is converted to dissolved inorganic carbon
 274 (DIC) in each box. The new DIC values are used within the chemistry submodel to
 275 calculate pCO₂ values at the next time step.

276 **3.1 Adaptive-time step solver**

277 The fundamental time step in Hector is currently one year, and most model
278 components are solved at this resolution. The carbon cycle, however, operates on a
279 variable time step, ensuring accurate ODE solutions, even under high-emissions
280 scenarios. This will also allow future sub-annual applications where desired. The
281 adaptive time step accomplished using the *gsl_odeiv2_evolve_apply* solver package of
282 GSL 1.16, which varies the time step to keep truncation error within a specific tolerance
283 when advancing the model. Thus all the carbon cycle components handle indeterminate
284 time steps less than or equal to 1 year, and can signal the solver if a too-large time step
285 is leading to instability. The solver then re-retries the solution, using a series of smaller
286 steps. From the coupler’s point of view, however, the entire model continues to
287 advance in annual increments.

288 **4.0 Other Components**

289 **4.1 Global Atmospheric Temperature**

290 Near surface global atmospheric temperature is calculated by:

$$\Delta T(t) = \lambda * RF(t) - F_H(t) \quad (13)$$

291 where the user-specified λ is the climate feedback parameter, defined as $\lambda = S'/S$, S' is
292 the climate sensitivity parameter (3 K) and S is the equilibrium climate sensitivity for a
293 doubling of CO_2 (3.7 W m^{-2}) (Knutti and Hegerl, 2008). RF is the total radiative forcing
294 and F_H is the ocean heat flux. F_H is calculated by a simple sigmoidal expression of the
295 ocean heat uptake efficiency k ($\text{W m}^{-2} \text{ K}^{-1}$) that decreases with increasing global

296 temperatures) multiplied by the atmospheric temperature change prior to the ocean's
297 removal of heat from the atmosphere (T_H) (Raper et al., 2002).

$$\Delta F_H(t) = k * \Delta T_H(t) \quad (14)$$

298 As global temperatures rise, the uptake capacity of the ocean may diminish, simulating
299 both a saturation of heat in the surface and a slowdown in ocean circulation with
300 increased temperatures. Finally, the temperature effects from atmospheric $[CO_2]$ are
301 lagged in time, as there are numerous real-world processes not simulated in Hector
302 buffering the temperature effects of increasing atmospheric $[CO_2]$.

303 **4.2 Radiative Forcing**

304 Radiative forcing is calculated from a series of atmospheric greenhouse gases,
305 aerosols, and pollutants (**Eq. 15-16, 18-22, 25, 29-30**). Radiative forcing is reported as
306 the relative radiative forcing. The base year user-specified forcings are subtracted from
307 the total radiative forcing to yield a forcing relative to the base year (1750).

308 **4.2.1. CO₂**

309 Radiative forcing from atmospheric $[CO_2]$ in $W m^{-2}$ is calculated based on
310 Meinshausen et al. (2011a):

$$RF_{CO_2} = 5.35 * \log \frac{Ca}{C0} \quad (15)$$

311 where, $5.35 W m^{-2}$ is a scaling parameter from Myhre et al. (1998), Ca is the
312 current atmospheric $[CO_2]$ in ppmv and $C0$ is the preindustrial $[CO_2]$ in ppmv.

313 **4.2.2 Halocarbons**

314 The halocarbon component of the model can accept an arbitrary number of gas
315 species, each characterized by a name, a lifetime τ (yr), a radiative forcing efficiency α

316 ($W m^{-2} pptv^{-1}$), an optional user-specified preindustrial concentration (pptv), and a
 317 molar mass (g). For each gas, its concentration (C_i) at time t is then computed based on
 318 a specified emissions time series E , assuming an exponential decay from the
 319 atmosphere:

$$C(t) = C_0 * \exp\left(-\frac{1}{T}\right) + E * T * \left(1 - \exp\left(-\frac{1}{T}\right)\right) \quad (16)$$

321 E is corrected for atmospheric dry air mole constant (1.8) and the molar mass of each
 322 halocarbon. The default model input files include these parameters and a time series of
 323 emissions for C2F6, CCl4, CF4, CFC11, CFC12, CFC113, CFC114, CFC115, CH3Br, CH3CCl3,
 324 CH3Cl, HCF22, HCF141b, HCF142b, HFC23, HFC32, HFC125, HFC134a, HFC143a,
 325 HFC227ea, HFC245ca, HFC245fa, HFC4310, SF6, halon1211, halon1301, and halon2402.

326 Radiative forcing by halocarbons, and other gases controlled under the Montreal
 327 Protocol, SF₆, and ozone are calculated via:

$$RF = \alpha [C(t)] \quad (17)$$

328 where α is the radiative efficiency (input parameters) in $W m^{-2} ppbv^{-1}$, and C is the
 329 atmospheric concentration.

330 **4.2.3 Ozone**

331 Tropospheric ozone concentrations are calculated from the CH₄ concentration
 332 and the emissions of three primary pollutants: NO_x, CO, and NMVOCs, modified from
 333 Tanaka et al. (2007a):

$$O_{3t} = (5.0 * \ln[CH_4]) + (0.125 * ENO_x) + (0.0011 * ECO) \quad (18)$$

$$+ (0.0033 * EVOC)$$

334 where the constants are the ozone sensitivity factors for each of the precursors (Ehhalt
 335 et al., 2001). The radiative forcing of tropospheric ozone is calculated from a linear
 336 relationship using a radiative efficiency factor (Joos et al., 2001a):

$$RF_{O_3} = 0.042 * [O_3] \quad (19)$$

339 **4.2.4 BC and OC**

340 The radiative forcing from black and organic carbon is a function their emissions (*EBC*
 341 and *EOC*).

$$RF_{BC} = 0.0743 \text{ Wm}^{-2}\text{Tg}^{-1} * EBC \quad (20)$$

$$RF_{OC} = -0.0128 \text{ Wm}^{-2}\text{Tg}^{-1} * EOC \quad (21)$$

342 The coefficients include both indirect and direct forcings of black and organic carbon
 343 (fossil fuel and biomass) (Bond et al., 2013, table C1).

344 **4.2.5 Sulphate Aerosols**

345 The radiative forcing from sulphate aerosols is a combination of the direct and indirect
 346 forcings (Joos et al., 2001a).

$$RF_{SOx \text{ Direct}} = -0.35 \text{ Wm}^{-2} * \frac{ESO_{x_t}}{ESO_{x_{t0}}} \quad (22)$$

$$RF_{SOx \text{ Indirect}} = -0.6 \text{ Wm}^{-2} * \frac{(\ln(ESN) + EeSO_{x_t})}{ESN} \quad (23)$$

$$* \left(\ln \frac{ESN + EeSO_{x_{t0}}}{ESN} \right)^{-1}$$

347 The direct forcing by sulphate aerosols is proportional to the anthropogenic sulphur
 348 emissions (GgS yr^{-1}) divided by the sulphate emissions from 2000. The indirect forcing by
 349 sulphate aerosols is a function of the anthropogenic and natural sulphur emissions.

350 Natural sulphur emissions, denoted by ESN , are equal to 42000 Gg S. A time series of
 351 annual mean volcanic stratospheric aerosol forcing ($W m^{-2}$) is supplied from
 352 Meinshausen et al. (2011b) and added to the indirect and direct forcing for a total
 353 sulphate forcing.

354 **4.2.6 Methane (CH_4)**

355 The change in $[CH_4]$ is calculated directly from CH_4 emissions, and sinks of CH_4 in the the
 356 troposphere (based on the lifetime of OH), stratosphere, and soil based on Wigley et al.
 357 (2002).

$$\Delta CH_4 = \frac{E(CH_4)}{2.78} - \frac{[CH_4]}{T_{OH}} - \frac{[CH_4]}{T_{strat}} - \frac{[CH_4]}{T_{soil}} \quad (24)$$

358 where E is total CH_4 emissions ($Tg yr^{-1}$) from both natural and anthropogenic sources,
 359 2.78 ($Tg ppb^{-1}$) is the conversion factor, and T are the lifetimes of the tropospheric sink
 360 (T_{OH}), the stratospheric sink ($T_{strat} = 120$ year), and the soil sink ($T_{soil} = 160$ year). Note
 361 that within Hector, natural emissions are held at a constant $300 Tg yr^{-1}$.

362 The lifetime of OH is a function of $[CH_4]$, and the emissions of NO_x , CO and VOC,
 363 based on Tanaka et al. (2007a).

$$\begin{aligned} \ln(OH)_t = & -0.32 (\ln[CH_4]_t - \ln[CH_4]_{t0}) + 0.0042 (E(NO_x)_t \\ & - (E(NO_x)_{t0}) - 0.000105 (E(CO)_t - (E(CO)_{t0}) \\ & - 0.00315 (E(VOC)_t - (E(VOC)_{t0})) \end{aligned} \quad (25)$$

364 The radiative forcing equation for CH_4 (Joos et al., 2001a) is a function of the
 365 concentrations (ppbv) of both CH_4 and N_2O :

$$RF_{CH_4} = 0.036 Wm^{-2} \left[\sqrt{[CH_4](t)} - \sqrt{[CH_4](t_0)} \right] \quad (26)$$

$$- f[CH_4(t), N_2O(t_0)] - f[CH_4(t_0), N_2O(t_0)]$$

366 The function f accounts for the overlap in CH_4 and N_2O in their bands is:

$$f(M, N) = 0.47 \quad (27)$$

$$* \ln(1 + (2.01 * 10^{-5}) * (MN)^{0.75} + (5.31 * 10^{-15}) * M$$

$$* (MN)^{1.52})$$

367 **4.2.7 N₂O**

368 The change in $[N_2O]$ is a function of N_2O emissions, and the lifetime of N_2O based on

369 Ward and Mahowald (2014).

$$\Delta N_2O = \frac{E(N_2O)}{4.8} - \frac{[N_2O]}{T_{N_2O}} \quad (28)$$

370 where E is total N_2O emissions ($Tg N yr^{-1}$), both natural and anthropogenic, 4.8 ($Tg N$

371 $ppbv^{-1}$) is the conversion factor, and T_{N_2O} is the lifetime of N_2O . We set natural

372 emissions of N_2O to linearly decrease from 11 $Tg N yr^{-1}$ in 1765, to 8 $Tg N yr^{-1}$ in 2000

373 and are then held constant at 8 $Tg N yr^{-1}$ to 2300. The lifetime of N_2O is a function of its

374 initial lifetime (T_0) and concentration ($[N_2O]_{t_0}$).

$$T_{N_2O} = T_0 * \left(\frac{[N_2O]_t}{[N_2O]_{t_0}} \right)^{-0.05} \quad (29)$$

375 The radiative forcing equation for N_2O (Joos et al., 2001a) is a function of the

376 concentration (ppbv) of both CH_4 and N_2O :

$$RF_{N_2O} = 0.12 Wm^{-2} \left[\sqrt{[N_2O]_t} - \sqrt{[N_2O]_{t_0}} \right] - f[CH_4(t_0), N_2O(t)] \quad (30)$$

$$- f[CH_4(t_0), N_2O(t_0)]$$

377 The function f accounts for the overlap in CH₄ and N₂O in their bands is the same as
378 equation 27.

379 **4.2.8 Stratospheric H₂O from CH₄ oxidation:**

380 The radiative forcing from stratospheric H₂O is a function of the [CH₄] (Tanaka et al.,
381 2007a). The coefficient 0.05 is from Joos et al. (2001a) based on the fact that the forcing
382 contribution from stratospheric H₂O is about 5% of the total CH₄ forcing (IPCC, 2001).
383 The 0.036 value of the coefficient corresponds to the same value used in the CH₄
384 radiative forcing equation.

$$RF_{stratH2O} = 0.05 * \left\{ 0.036 \text{ Wm}^{-2} * \left(\sqrt{[CH_4]_t} - \sqrt{[CH_4]_{t0}} \right) \right\} \quad (31)$$

385

386 **5.0 Model Experiments and Data Sources**

387 A critical test of Hector's performance is to compare the major climatic variables
388 calculated in Hector, e.g., atmospheric [CO₂], radiative forcing, and atmospheric
389 temperature, to observational records and both simple and complex climate models.
390 Within this study, Hector is run under prescribed emissions from 1850 to 2300 for all
391 four Representative Concentration Pathways (RCPs), freely available at
392 <http://tntcat.iiasa.ac.at/RcpDb/> (Moss et al., 2010; van Vuuren et al., 2007; Clarke et al.,
393 2007; Wise et al., 2009; Riahi et al., 2007; Fujino et al., 2006; Hijioka et al., 2008; Smith
394 and Wigley, 2006). The RCPs are plausible future scenarios that were developed to
395 improve our understanding of the coupled human climate system. RCPs by definition

396 are concentration pathways; however, for all experiments within this manuscript we use
397 the corresponding emissions trajectories from each RCP as input for Hector.

398 Comparison data was obtained from a series of models. We compared Hector
399 results to MAGICC, a SCM widely used in the scientific and IAM communities, for global
400 variables such as atmospheric CO₂, radiative forcing, and temperature (e.g., Raper et al.,
401 2001; Wigley, 1995; Meinshausen et al., 2011a). We also compare Hector to a suite of
402 eleven Earth System Models included in the 5th Coupled Model Intercomparison Project
403 (CMIP5) archive (Taylor et al., 2012) (**Table 3**). All CMIP5 data were converted to yearly
404 global averages from the historical period through the RCPs and their extensions. One
405 standard deviation of the annual global averages and the CMIP5 model range were
406 calculated for each variable using the RCMIP5 (<http://github.com/JGCRI/RCMIP5>)
407 package in R. All CMIP5 variables used in this study are from model runs with
408 prescribed atmospheric concentrations, except for comparisons involving atmospheric
409 [CO₂] which are from the emissions driven scenario (esmHistorical and esmRCP8.5)
410 (Figures 3 and 5). We acknowledge that this comparison, between an emissions-forced
411 model (Hector) and concentration-forced models (CMIP5), is not perfect. However, very
412 few CMIP5 models were run under prescribed emissions scenarios.

413 We compare Hector to observations of atmospheric [CO₂] from Law Dome
414 (1010-1975) and Mauna Loa (1958 – 2008), (Keeling and Whorf, 2005; Etheridge et al.,
415 1996). Global temperature anomalies are from HadCRUT4 (Morice et al., 2012).
416 Observations of air-sea and air-land fluxes are from the Global Carbon Project (GCP) (Le
417 Quéré et al., 2013). Lastly, observations of surface ocean pH are from Bermuda Atlantic

418 Time Series (BATS) and Hawaii Ocean Time Series (HOTS) (Bates, 2007; Fujieki et al.,
419 2013).

420

421 **6.0 Results and Discussion**

422 **6.1 Historical**

423 A critical test of Hector's performance is how well it compares to historical and
424 present day climate from observations, MAGICC, and a suite of CMIP5 models. Rates of
425 change and root mean square errors were calculated for Hector's primary outputs,
426 which are summarized in **Table 4**. After spinup is complete in Hector, atmospheric [CO₂]
427 in 1850 is 286.0 ppmv, which compares well with observations from Law Dome of 285.2
428 ppmv. Hector captures the global trends in atmospheric [CO₂] (**Figure 3**) with an
429 average root mean square error (RMSE) of 2.85 ppmv (**Table 4a**), when compared to
430 observations, MAGICC6, and CMIP5 data from 1850-2005. Rate of change of
431 atmospheric [CO₂] from 1850-2005 is slightly lower than the observations, MAGICC6,
432 and CMIP5. Hector can be forced to match atmospheric [CO₂] records (section 2.4), but
433 we disabled this feature to highlight the full performance of the model. Note however,
434 that in the MAGICC6 results a similar feature was used to force the output to match the
435 historical atmospheric [CO₂] record.

436 Historical global atmospheric temperature anomalies (relative to 1850) are
437 compared across Hector, MAGICC6, CMIP5, and observations from HadCRUT4 (**Figure**
438 **4**). Atmospheric temperature change from Hector (0.98 °C) over the period 1850 to
439 2005 closely match the CMIP5 temperature change (1.01 °C), both slightly higher than

440 the observational record. Over this time period a Hector has an average RMSE of 0.14
441 °C. Note that simple climate models do not aim to capture temperature variations due
442 to interannual/decadal variability found in ESMs or the real world; instead they simulate
443 the overall trends in global mean temperature change.

444 **6.2 Future Projections**

445 Hector's strengths lie within policy relevant time scales of decades to centuries,
446 and here we compare Hector to MAGICC and CMIP5 under differing future climate
447 projections. Results from all four RCPs are broadly similar when comparing Hector, to
448 MAGICC6, and CMIP5; we display here RCP8.5 results as representative. Studies suggest
449 that 80% of the anthropogenic CO₂ emissions have an average atmospheric lifetime of
450 300-450 years (Archer et al., 1997; Rogner, 1997; Archer, 2005). Hector has all the
451 necessary components to model the climate system from present day through the next
452 approximately 300 years. **Figure 5** highlights historical trends in atmospheric [CO₂],
453 along with projections of atmospheric [CO₂] under esmRCP8.5 from 1850 to 2100. Note
454 that the emissions forced scenario only extends to 2100 and not to 2300 like the
455 concentration forced scenarios (e.g., Figure 8). Both Hector and MAGICC6 are on the
456 low end of the CMIP5 median, but fall within one standard deviation and model range,
457 with a RMSE of 9.0 ppmv (**Table 4b**).

458 The CMIP5 archive does not provide emissions prescribed scenarios for all RCPs;
459 we can only compare atmospheric [CO₂] from Hector with MAGICC6 under all four RCP
460 scenarios out to 2300 (**Figure 6**). Hector's change in [CO₂] (1472.13 ppmv) from 1850 to
461 2300 is slightly lower than MAGICC6 (1600.0 ppmv) for RCP 8.5. This is most likely due

462 to different representations of the global carbon cycle. We compare Hector to
463 MAGICC6 for changes in radiative forcing under the four RCPs (**Figure 7**). Radiative
464 forcing was not provided within the CMIP5 archive and therefore we can only compare
465 Hector and MAGICC6. Over the period 1850 to 2300 Hector (12.80 Wm^{-2}) and MAGICC6
466 (12.24 Wm^{-2}) are comparable in their change in radiative forcing, with a RMSE of 0.26 W
467 m^{-2} . One noticeable difference between MAGICC6 and Hector during the historical
468 period is the decreases in radiative forcing. This is due to the effects of volcanic
469 emissions on radiative forcing. For simplicity, we have chosen to run Hector without
470 these effects.

471 **Figure 8** compares global temperature anomalies from Hector to MAGICC6 and
472 CMIP5 over the four RCPs, from 2005 to 2300. Hector simulates the CMIP5 median
473 more closely than MAGICC6 across all four RCPs, with a temperature change under RCP
474 8.5 for Hector of $8.59 \text{ }^{\circ}\text{C}$, compared to MAGICC6 of $7.30 \text{ }^{\circ}\text{C}$, while the temperature
475 change for CMIP5 is $9.57 \text{ }^{\circ}\text{C}$ (**Table 4c**). To highlight this close comparison, temperature
476 change over the entire record (1850-2300) for Hector is $9.58 \text{ }^{\circ}\text{C}$, which is within $1.0 \text{ }^{\circ}\text{C}$ of
477 the CMIP5 median, while MAGICC6's temperature change is greater than $2.5 \text{ }^{\circ}\text{C}$ away
478 from the CMIP5 median.

479 **Figures 9 and 10** present a detailed view of carbon fluxes under RCP 8.5, for
480 CMIP5 and observations (negative represents carbon flux to the atmosphere). The
481 ocean is a major sink of carbon through 2100, becoming less effective with time in both
482 Hector and the CMIP5 models. MAGICC6 does not include air-sea fluxes in its output,
483 and because it is not open source we were unable to obtain these values. Therefore, we

484 compare air-sea fluxes of CO₂ to MAGICC5.3, updated with explicit BC and OC forcing as
485 described in Smith and Bond (2014). Hector's calculation of air-sea fluxes is within the
486 large CMIP5 model range up to 2100. However, after that Hector peaks close to 2150,
487 while the CMIP5 models are beginning to decline. One potential reason for this
488 discrepancy after 2100 is that in this version of Hector, we do not simulate changes in
489 ocean circulation, potentially biasing fluxes too high after 2100. Most ESMs in CMIP5
490 show a weakening of the Atlantic meridional overturning circulation by 2100 between
491 15% and 60% under RCP 8.5 (Cheng et al., 2013). A slowdown in ocean circulation may
492 result in less carbon uptake by the oceans. Another potential reason for this bias is
493 Hector's constant pole to equator ocean temperature gradient. Studies show that the
494 Arctic is warming faster than the rest of the globe (e.g., Bintanja and van der Linden,
495 2013; Holland and Bitz, 2003; Bekryaev et al., 2010). A warmer high latitude surface
496 ocean in Hector would suppress the uptake of carbon, potentially bringing the air-sea
497 fluxes closer to the CMIP5 median after 2100.

498 CMIP models tend to show huge divergences in their land responses to changing
499 climate (e.g., Friedlingstein et al., 2006), which is evident by the large range in CMIP5
500 models (**Figure 10**). Hector simulates the general trends, of increasing carbon sink and
501 then a gradual decline to a carbon source after 2100. Both land and ocean fluxes within
502 Hector agree well the observations from Le Queré et al., (2013).

503 One feature in Hector that is unique amongst SCMs is its ability to actively solve
504 the carbonate system in the upper ocean (Hartin et al, in prep). This feature allows us
505 to predict changes ocean acidification, calcium carbonate saturations and other

506 carbonate system parameters. **Figure 11** shows low latitude (<55°) pH for Hector
507 compared to CMIP5 and observations from 1850 to 2100 under RCP 8.5. The model
508 projects a significant drop in pH from present day through 2100, which may lead to
509 detrimental effects on marine ecosystems (e.g., Fabry et al., 2008).

510

511 **7.0 Conclusions**

512 Hector reproduces the large-scale couplings and feedbacks on the climate
513 system between the atmosphere, ocean, and land, falling within the range of the CMIP5
514 model and matching MAGICC. It does not simulate the fine details or parameterizations
515 found in large-scale, complex ESMs, but instead represents the most critical global
516 processes in a reduced-complexity form. This allows for fast execution times, ease of
517 understanding, and straightforward analysis of the model output.

518 Two of Hector's key features are its open source nature and modular design.
519 This allows the user to edit the input files and code at will, for example to
520 enable/disable/replace components, or include components not found within the core
521 version of Hector. For example, a user can design a new submodel (e.g., sea-ice) to
522 answer specific climate questions relating to that process. Hector is hosted on a widely-
523 used open source software repository (Github), and thus changes and improvements
524 can be easily shared with the scientific community. Because of these critical features,
525 Hector has the potential to be a key analytical tool in both the policy and scientific
526 communities. We welcome user input and encourage use, modifications, and
527 collaborations with Hector.

528 While Hector has many strengths, the current 1.0 version has some limitations.
529 For example, Hector does not currently simulate terrestrial gross primary production, a
530 key metric of comparison to e.g. the FLUXNET database. Also, Hector does not have
531 differential radiative forcing and atmospheric temperature calculations over land and
532 ocean. This may be a problem, as land responds to changes in emissions of greenhouse
533 gases and aerosols much quicker than the ocean (Hansen et al., 2005). Hector does not
534 explicitly deal with oceanic heat uptake, except via a simple empirical formula. Surface
535 temperatures are calculated based on a linear relationship with atmospheric
536 temperature and we assume a constant pole to equator temperature gradient. We
537 acknowledge that this assumption may not hold true if the poles warm faster than the
538 equator.

539 Future plans with Hector include addressing some of the above limitations and
540 conducting numerous scientific experiments, using Hector as a stand-alone simple
541 climate carbon-cycle model. It is also being incorporated into Pacific Northwest
542 National Laboratory's Global Change Assessment Model for policy-relevant experiments.
543 Hector has the ability to be a key analytical tool used across many scientific and policy
544 communities due to its modern software architecture, open source, and object-oriented
545 structure.

546

547 **Code Availability**

548 Hector is freely available at <https://github.com/JGCRI/hector> . The specific Hector v1.0
549 referenced in this paper, as well as code to reproduce all figures and results shown here,
550 is available at <https://github.com/JGCRI/hector/releases/tag/v1.0>

551 **Author contributions**

552 C.A.H. and B.P.B.-L. developed the ocean and terrestrial carbon models, respectively,
553 and led the overall development of Hector. R.P.L. and P.P. wrote critical code for
554 Hector’s coupler and carbon cycle solver. A.S. helped with the development of the
555 atmospheric forcing components. C.A.H. wrote the manuscript with contributions from
556 all co-authors.

557

558 **Acknowledgements**

559 This research is based on work supported by the U.S. Department of Energy, Office of
560 Science, Integrated Assessment Research Program. The Pacific Northwest National
561 Laboratory is operated for DOE by Battelle Memorial Institute under contract DE-AC05-
562 76RL01830.

563 **References:**

- 564 Anthoff, D., and Tol, R. S. J.: The income elasticity of the impact of climate change, Is
565 the Environment a Luxury? An inquiry into the relationship between environment and
566 income, edited by: Tiezzi, S., and Martini, C., Routledge, 2014.
- 567 Applegate, P. J., Kirchner, N., Stone, E. J., Keller, K., and Greve, R.: An assessment of
568 key model parametric uncertainties in projections of Greenland Ice Sheet behavior, *The*
569 *Cryosphere*, 6, 589-606, 10.5194/tc-6-589-2012, 2012.
- 570 Archer, D., Kheshgi, H., and Maier-Reimer, E.: Multiple timescales for neutralization of
571 fossil fuel CO₂, *Geophysical Research Letters*, 24, 405-408, 10.1029/97GL00168, 1997.
- 572 Archer, D.: Fate of fossil fuel CO₂ in geologic time, *Journal of Geophysical Research:*
573 *Oceans*, 110, C09S05, 10.1029/2004JC002625, 2005.
- 574 Bates, N. R.: Interannual variability of the oceanic CO₂ sink in the subtropical gyre of the
575 North Atlantic Ocean over the last 2 decades, *Journal of Geophysical Research: Oceans*,
576 112, C09013, 10.1029/2006JC003759, 2007.
- 577 Bekryaev, R. V., Polyakov, I. V., and Alexeev, V. A.: Role of Polar Amplification in
578 Long-Term Surface Air Temperature Variations and Modern Arctic Warming, *Journal of*
579 *Climate*, 23, 3888-3906, 10.1175/2010JCLI3297.1, 2010.
- 580 Bintanja, R., and van der Linden, E. C.: The changing seasonal climate in the Arctic, *Sci.*
581 *Rep.*, 3,
582 [http://www.nature.com/srep/2013/130327/srep01556/abs/srep01556.html#supplementary](http://www.nature.com/srep/2013/130327/srep01556/abs/srep01556.html#supplementary-information)
583 [-information](http://www.nature.com/srep/2013/130327/srep01556/abs/srep01556.html#supplementary-information), 2013.
- 584 Bond-Lamberty, B., Calvin, K., Jones, A. D., Mao, J., Patel, P., Shi, X., Thomson, A.,
585 Thornton, P., and Zhou, Y.: Coupling earth system and integrated assessment models: the
586 problem of steady state, *Geosci. Model Dev. Discuss.*, 7, 1499-1524, 10.5194/gmdd-7-
587 1499-2014, 2014.
- 588 Bond, T. C., Doherty, S. J., Fahey, D. W., Forster, P. M., Berntsen, T., DeAngelo, B. J.,
589 Flanner, M. G., Ghan, S., Kärcher, B., Koch, D., Kinne, S., Kondo, Y., Quinn, P. K.,
590 Sarofim, M. C., Schultz, M. G., Schulz, M., Venkataraman, C., Zhang, H., Zhang, S.,
591 Bellouin, N., Guttikunda, S. K., Hopke, P. K., Jacobson, M. Z., Kaiser, J. W., Klimont,
592 Z., Lohmann, U., Schwarz, J. P., Shindell, D., Storelvmo, T., Warren, S. G., and Zender,
593 C. S.: Bounding the role of black carbon in the climate system: A scientific assessment,
594 *Journal of Geophysical Research: Atmospheres*, 118, 5380-5552, 10.1002/jgrd.50171,
595 2013.
- 596 Bouwman, A. F., Hoek, K. W. v. d., Drecht, G. V., and Eickhout, B.: World Livestock
597 and crop production systems, land use and environment between 1970 and 2030, *Rural*
598 *Lands, Africulture and Climate beyond 2015: A new prespective on suture land use*
599 *patterns*, edited by: Brouwer, F., and McCarl, B., Springer, Dordrecht, 2006.
- 600 Calvin, K., Clarke, L., Edmonds, J., Eom, J., Hejazi, M., Kim, S., Kyle, G., Link, R.,
601 Patel, P., Smith, S., and Wise, M.: GCAM Wiki Documentation, PNNL-20809, Pacific
602 Northwest National Laboratory, Richland WA, 2011.
- 603 Castruccio, S., McInerney, D. J., Stein, M. L., Crouch, F. L., Jacob, R. L., and Moyer, E.
604 J.: Statistical Emulation of Climate Model Projections Based on Precomputed GCM
605 Runs, *Journal of Climate*, 27, 2014.

606 Challenor, P.: Using emulators to estimate uncertainty in complex models, *Uncertainty*
607 *Quantification in Scientific Computing*, edited by: Dienstry, A. M., and Boisvert, R. F.,
608 Springer, IFIP AICT 377, 151-164 pp., 2012.

609 Cheng, W., Chiang, J. C. H., and Zhang, D.: Atlantic Meridional Overturning Circulation
610 (AMOC) in CMIP5 Models: RCP and Historical Simulations, *Journal of Climate*, 26,
611 7187-7197, 10.1175/JCLI-D-12-00496.1, 2013.

612 Clarke, L., J. Edmonds, H. Jacoby, H. Pitcher, Reilly, J., and Richels, R.: Scenarios of
613 Greenhouse Gas Emissions and Atmospheric Concentrations. Sub-report 2.1A of
614 Synthesis and Assessment Product 2.1, edited by: Research, U. S. C. C. S. P. a. t. S. o. G.
615 C., Department of Energy, Office of Biological & Environmental Research, Washington,
616 7 DC., USA, 2007.

617 Collins, W. D., Craig, A. P., Truesdale, J. E., Di Vittorio, A. V., Jones, A. D., Bond-
618 Lamberty, B., Calvin, K. V., Edmonds, J. A., Kim, S. H., Thomson, A. M., Patel, P.,
619 Zhou, Y., Mao, J., Shi, X., Thornton, P. E., Chini, L. P., and Hurtt, G. C.: The integrated
620 Earth System Model (iESM): formulation and functionality, *Geosci. Model Dev.*
621 *Discuss.*, 8, 381-427, 10.5194/gmdd-8-381-2015, 2015.

622 Denman, K. L., G. Brasseur, A. Chidthaisong, P. Ciais, P.M. Cox, R.E. Dickinson, D.
623 Hauglustaine, C. Heinze, E. Holland, D. Jacob, U. Lohmann, S Ramachandran, P.L. da
624 Silva Dias, S.C. Wofsy and X. Zhang: *Climat Change 2007: The Physical Science Basis.*,
625 edited by: Change, C. o. W. G. I. t. t. F. A. R. o. t. I. P. o. C., Cambridge University
626 Press, Cambridge , United Kingdom and New York, USA, 2007.

627 Di Vittorio, A. V., Chini, L. P., Bond-Lamberty, B., Mao, J., Shi, X., Truesdale, J., Craig,
628 A., Calvin, K., Jones, A., Collins, W. D., Edmonds, J., Hurtt, G. C., Thornton, P., and
629 Thomson, A.: From land use to land cover: restoring the afforestation signal in a coupled
630 integrated assessment–earth system model and the implications for CMIP5 RCP
631 simulations, *Biogeosciences*, 11, 6435-6450, 10.5194/bg-11-6435-2014, 2014.

632 E.P. White, E. B., Z.T. Brym, K.J. Locey, D.J. McGlenn: Nine simple ways to make it
633 easier to (re)use your data, *PeerJ PrePrints*, 1:e7v2,
634 <http://dx.doi.org/10.7287/peerj.preprints.7v2>, 2013.

635 Edmonds, J., and Smith, S. J.: *The Technology of Two Degrees. Avoiding Dangerous*
636 *Climate Change*, edited by: Schellnhuber, H. J., Cramer, W., Nakicenovic, N., Wigley,
637 T., and Yohe, G., Cambridge University Press, Cambridge, UK, 2006.

638 Ehhalt, D., Prather, M. J., Dentener, F. J., Derwent, R., Dlugokencky, E. J., Holland, E.
639 A., Isaksen, I. S., Katima, J., Kirchoff, V., Matson, P. A., and Wang, M.: Atmospheric
640 chemistry and greenhouse gases, in: *Climate Change 2001: The Scientific Basis*, edited
641 by: Houghton, J. T., Ding, Y., Griggs, D. J., Noguer, M., van der Linden, L., Dai, X.,
642 Maskell, K., and Johnson, C. A., Cambridge University Press, Cambridge, UK, 892,
643 2001.

644 Etheridge, D. M., Steele, L. P., Langenfelds, R. L., Francey, R. J., Barnola, J. M., and
645 Morgan, V. I.: Natural and anthropogenic changes in atmospheric CO₂ over the last 1000
646 years from air in Antarctic ice and firn, *Journal of Geophysical Research: Atmospheres*,
647 101, 4115-4128, 10.1029/95JD03410, 1996.

648 Fabry, V. J., Seibel, B. A., Feely, R. A., and Orr, J. C.: Impacts of ocean acidification on
649 marine fauna and ecosystem processes, *ICES Journal of Marine Science: Journal du*
650 *Conseil*, 65, 414-432, 10.1093/icesjms/fsn048, 2008.

651 Friedlingstein, P., Cox, P., Betts, R., Bopp, L., von Bloh, W., Brovkin, V., Cadule, P.,
652 Doney, S., Eby, M., Fung, I., Bala, G., John, J., Jones, C., Joos, F., Kato, T., Kawamiya,
653 M., Knorr, W., Lindsay, K., Matthews, H. D., Raddatz, T., Rayner, P., Reick, C.,
654 Roeckner, E., Schnitzler, K. G., Schnur, R., Strassmann, K., Weaver, A. J., Yoshikawa,
655 C., and Zeng, N.: Climate–Carbon Cycle Feedback Analysis: Results from the C4MIP
656 Model Intercomparison, *Journal of Climate*, 19, 3337-3353, 10.1175/JCLI3800.1, 2006.
657 Friedlingstein, P., Meinshausen, M., Arora, V. K., Jones, C. D., Anav, A., Liddicoat, S.
658 K., and Knutti, R.: Uncertainties in CMIP5 Climate Projections due to Carbon Cycle
659 Feedbacks, *Journal of Climate*, 27, 511-526, 10.1175/JCLI-D-12-00579.1, 2014.
660 Fujieki, L., Santiago-Mandujano, F., Fumar, C., Liukas, R., and Church, M.: Hawaii
661 Ocean Time-series Program Data Report, 2013.
662 Fujino, J., Nair, R., Kainuma, M., Masui, T., and Matsuoka, Y.: Multi-gas mitigation
663 analysis on stabilization scenarios using AIM global model, *Multigas Mitigation and
664 Climate Policy*. The Energy Journal, Special Issue, 2006.
665 Hansen, J., Sato, M., Ruedy, R., Nazarenko, L., Lacis, A., Schmidt, G. A., Russell, G.,
666 Aleinov, I., Bauer, M., Bauer, S., Bell, N., Cairns, B., Canuto, V., Chandler, M., Cheng,
667 Y., Del Genio, A., Faluvegi, G., Fleming, E., Friend, A., Hall, T., Jackman, C., Kelley,
668 M., Kiang, N., Koch, D., Lean, J., Lerner, J., Lo, K., Menon, S., Miller, R., Minnis, P.,
669 Novakov, T., Oinas, V., Perlwitz, J., Perlwitz, J., Rind, D., Romanou, A., Shindell, D.,
670 Stone, P., Sun, S., Tausnev, N., Thresher, D., Wielicki, B., Wong, T., Yao, M., and
671 Zhang, S.: Efficacy of climate forcings, *Journal of Geophysical Research: Atmospheres*,
672 110, D18104, 10.1029/2005JD005776, 2005.
673 Hartin, C. A., Bond-Lamberty, B., and Patel, P.: Projections of ocean acidification over
674 three centuries using a carbonate chemistry box model, *Biogeosciences*, in prep.
675 Harvey, L. D. D., and Schneider, S. H.: Transient climate response to external forcing on
676 100–104 year time scales part 1: Experiments with globally averaged, coupled,
677 atmosphere and ocean energy balance models, *Journal of Geophysical Research:*
678 *Atmospheres*, 90, 2191-2205, 10.1029/JD090iD01p02191, 1985.
679 Heron, M., Hanson, V., and Ricketts, I.: Open source and accessibility: advantages and
680 limitations, *Journal of Interaction Science*, 1, 2, 10.1186/2194-0827-1-2, 2013.
681 Hijioka, Y., Matsuoka, Y., Nishimoto, H., Masui, M., and Kainuma, M.: Global GHG
682 emissions scenarios under GHG concentration stabilization targets, *Journal of
683 Environmental Engineering*, 13, 97-108, 2008.
684 Hoffert, M. I., Callegari, A. J., and Hsieh, C.-T.: The Role of Deep Sea Heat Storage in
685 the Secular Response to Climatic Forcing, *J. Geophys. Res.*, 85, 6667-6679,
686 10.1029/JC085iC11p06667, 1980.
687 Holland, M. M., and Bitz, C. M.: Polar amplification of climate change in coupled
688 models, *Climate Dynamics*, 21, 221-232, 10.1007/s00382-003-0332-6, 2003.
689 Ince, D. C., Hatton, L., and Graham-Cumming, J.: The case for open computer programs,
690 *Nature*, 482, 485-488, 2012.
691 IPCC: *Climate Change 2001: The Science of Climate Change*. Contribution of Working
692 Group I to the Second Assessment Report of the Intergovernmental Panel on Climate
693 Change, Cambridge University Press, Cambridge, 2001.
694 Irvine, P. J., Sriviver, R. L., and Keller, K.: Tension between reducing sea-level rise and
695 global warming through solar-radiation management, *Nature Clim. Change*, 2, 97-100,

696 <http://www.nature.com/nclimate/journal/v2/n2/abs/nclimate1351.html#supplementary->
697 [information](http://www.nature.com/nclimate/journal/v2/n2/abs/nclimate1351.html#supplementary-), 2012.

698 Joos, F., Prentice, I. C., Sitch, S., Meyer, R., Hooss, G., Plattner, G.-K., Gerber, S., and
699 Hasselmann, K.: Global warming feedbacks on terrestrial carbon uptake under the
700 Intergovernmental Panel on Climate Change (IPCC) Emission Scenarios, *Global*
701 *Biogeochemical Cycles*, 15, 891-907, 10.1029/2000GB001375, 2001a.

702 Joos, F., Prentice, I. C., Sitch, S., Meyer, R., Hooss, G., Plattner, G.-K., Gerber, S., and
703 Hasselmann, K.: Global warming feedbacks on terrestrial carbon uptake under the
704 Intergovernmental Panel on Climate Change (IPCC) emission scenarios, *Global*
705 *Biochemical Cycles*, 15, 891-907, 2001b.

706 Knox, F., and McElroy, M. B.: Changes in Atmospheric CO₂: Influence of the Marine
707 Biota at High Latitude, *J. Geophys. Res.*, 89, 4629-4637, 10.1029/JD089iD03p04629,
708 1984.

709 Knutti, R., and Hegerl, G. C.: The equilibrium sensitivity of the Earth's temperature to
710 radiation changes, *Nature Geosci*, 1, 735-743, 2008.

711 Le Quéré, C., Andres, R. J., Boden, T., Conway, T., Houghton, R. A., House, J. I.,
712 Marland, G., Peters, G. P., van der Werf, G. R., Ahlström, A., Andrew, R. M., Bopp, L.,
713 Canadell, J. G., Ciais, P., Doney, S. C., Enright, C., Friedlingstein, P., Huntingford, C.,
714 Jain, A. K., Jourdain, C., Kato, E., Keeling, R. F., Klein Goldewijk, K., Levis, S., Levy,
715 P., Lomas, M., Poulter, B., Raupach, M. R., Schwinger, J., Sitch, S., Stocker, B. D.,
716 Viovy, N., Zaehle, S., and Zeng, N.: The global carbon budget 1959–2011, *Earth Syst.*
717 *Sci. Data*, 5, 165-185, 10.5194/essd-5-165-2013, 2013.

718 Lenton, T. M.: Land and ocean carbon cycle feedback effects on global warming in a
719 simple Earth system model, *Tellus B*, 52, 1159-1188, 10.1034/j.1600-0889.2000.01104.x,
720 2000.

721 Lenton, T. M., Myerscough, R. J., Marsh, R., Livina, V. N., Price, A. R., and Cox, S. J.:
722 Using GENIE to study a tipping point in the climate system, 1890, 871-884 pp., 2009.

723 Manne, A. S., and Richels, R. G.: Merge: an integrated assessment model for global
724 climate change, *Energy and environment*, edited by: Loulou, R., Waub, J.-P., and
725 Zaccour, G., Springer, New York, 2005.

726 Martin, R. C., Riehle, D., and Buschmann, F.: *Pattern Languages of Program Design 3*,
727 Addison-Wesley, Boston, MA, 672 pp., 1997.

728 Meinshausen, M., Raper, S. C. B., and Wigley, T. M. L.: Emulating coupled atmosphere-
729 ocean and carbon cycle models with a simpler model, *MAGICC6 – Part 1: Model*
730 *description and calibration*, *Atmos. Chem. Phys.*, 11, 1417-1456, 10.5194/acp-11-1417-
731 2011, 2011a.

732 Meinshausen, M., Smith, S. J., Calvin, K., Daniel, J. S., Kainuma, M. L. T., Lamarque, J.
733 F., Matsumoto, K., Montzka, S. A., Raper, S. C. B., Riahi, K., Thomson, A., Velders, G.
734 J. M., and Vuuren, D. P. P.: The RCP greenhouse gas concentrations and their extensions
735 from 1765 to 2300, *Climatic Change*, 109, 213-241, 10.1007/s10584-011-0156-z, 2011b.

736 Meinshausen, M., Wigley, T. M. L., and Raper, S. C. B.: Emulating atmosphere-ocean
737 and carbon cycle models with a simpler model, *MAGICC6 – Part 2: Applications*,
738 *Atmos. Chem. Phys.*, 11, 1457-1471, 10.5194/acp-11-1457-2011, 2011c.

739 Morice, C. P., Kennedy, J. J., Rayner, N. A., and Jones, P. D.: Quantifying uncertainties
740 in global and regional temperature change using an ensemble of observational estimates:

741 The HadCRUT4 data set, *Journal of Geophysical Research: Atmospheres*, 117, D08101,
742 10.1029/2011JD017187, 2012.

743 Moss, R. H., Edmonds, J. A., Hibbard, K. A., Manning, M. R., Rose, S. K., van Vuuren,
744 D. P., Carter, T. R., Emori, S., Kainuma, M., Kram, T., Meehl, G. A., Mitchell, J. F. B.,
745 Nakicenovic, N., Riahi, K., Smith, S. J., Stouffer, R. J., Thomson, A. M., Weyant, J. P.,
746 and Wilbanks, T. J.: The next generation of scenarios for climate change research and
747 assessment, *Nature*, 463, 747-756,
748 http://www.nature.com/nature/journal/v463/n7282/supinfo/nature08823_S1.html, 2010.

749 Murakami, K., Sasai, T., and Yamaguchi, Y.: A new one-dimensional simple energy
750 balance and carbon cycle coupled model for global warming simulation, *Theoretical and*
751 *Applied Climatology*, 101, 459-473, 10.1007/s00704-009-0232-8, 2010.

752 Myhre, G., Highwood, E. J., Shine, K. P., and Stordal, F.: New estimates of radiative
753 forcing due to well mixed greenhouse gases, *Geophysical Research Letters*, 25, 2715-
754 2718, 10.1029/98GL01908, 1998.

755 Nemani, R. R., Keeling, C. D., Hashimoto, H., Jolly, W. M., Piper, S. C., Tucker, C. J.,
756 Myneni, R. B., and Running, S. W.: Climate-Driven Increases in Global Terrestrial Net
757 Primary Production from 1982 to 1999, *Science*, 300, 1560-1563,
758 10.1126/science.1082750, 2003.

759 Nordhaus, W. D.: A question of balance weighing the options on global warming
760 policies, Yale University Press, New Haven, 2008.

761 Piao, S., Sitch, S., Ciais, P., Friedlingstein, P., Peylin, P., Wang, X., Ahlström, A., Anav,
762 A., Canadell, J. G., Cong, N., Huntingford, C., Jung, M., Levis, S., Levy, P. E., Li, J.,
763 Lin, X., Lomas, M. R., Lu, M., Luo, Y., Ma, Y., Myneni, R. B., Poulter, B., Sun, Z.,
764 Wang, T., Viovy, N., Zaehle, S., and Zeng, N.: Evaluation of terrestrial carbon cycle
765 models for their response to climate variability and to CO₂ trends, *Global Change*
766 *Biology*, 19, 2117-2132, 10.1111/gcb.12187, 2013.

767 Pietsch, S. A., and Hasenauer, H.: Evaluating the self-initialization procedure for large-
768 scale ecosystem models, *Global Change Biology*, 12, 1-12, 10.1111/j.1365-
769 2486.2006.01211.x 2006.

770 Raper, S. C., Gregory, J. M., and Stouffer, R. J.: The Role of Climate Sensitivity and
771 Ocean Heat Uptake on AOGCM Transient Temperature Response, *Journal of Climate*,
772 15, 124-130, 2002.

773 Raper, S. C. B., Gregory, J. M., and Osborn, T. J.: Use of an upwelling-diffusion energy
774 balance climate model to simulate and diagnose A/OGCM results, *Climate Dynamics*, 17,
775 601-613, 2001.

776 Ratto, M., Castelletti, A., and Pagano, A.: Emulation techniques for the reduction and
777 sensitivity analysis of complex environmental models, *Environmental Modelling and*
778 *Software*, 34, 1-4, 2012.

779 Riahi, K., Grubler, A., and Nakicenovic, N.: Scenarios of long-term socio-economic and
780 environmental development under climate stabilization, *Technological Forecasting and*
781 *Social Change*, 74, 887-935, 2007.

782 Ricciuto, D. M., Davis, K. J., and Keller, K.: A Bayesian calibration of a simple carbon
783 cycle model: The role of observations in estimating and reducing uncertainty, *Global*
784 *Biogeochemical Cycles*, 22, GB2030, 10.1029/2006GB002908, 2008.

785 Rogner, H. H.: An assessment of world hydrocarbon resources, *Annual Review of*
786 *Energy and the Environment*, 22, 217-262, 10.1146/annurev.energy.22.1.217, 1997.

787 Schlesinger, M. E., and Jiang, X.: Simple Model Representation of Atmosphere-Ocean
788 GCMs and Estimation of the Time Scale of CO₂-Induced Climate Change, *Journal of*
789 *Climate*, 3, 1297-1315, 10.1175/1520-0442(1990)003<1297:SMROAO>2.0.CO;2, 1990.
790 Senior, C. A., and Mitchell, J. F. B.: The time-dependence of climate sensitivity,
791 *Geophysical Research Letters*, 27, 2685-2688, 10.1029/2000GL011373, 2000.
792 Smith, S., and Wigley, T.: Multi-Gas Forcing Stabilization with the MiniCAM, *Energy*
793 *Journal Special Issue #3*, 373-391, 2006.
794 Smith, S. J., and Bond, T. C.: Two hundred fifty years of aerosols and climate: the end of
795 the age of aerosols, *Atmos. Chem. Phys. Discuss.*, 13, 6419-6453, 10.5194/acp-14-537-
796 2014, 2014.
797 Sokolov, A. P., CA, S., S, D., S, P., DW, K., HD, J., RG, P., CE, F., JM, R., C, W., B, F.,
798 MC, S., J, S., PH, S., M, J., and J, C.: The MIT Integrated Global System Model (IGSM)
799 version 2: model description and baseline evaluation, MIT, Cambridge, 2005.
800 Sriver, R., Urban, N., Olson, R., and Keller, K.: Toward a physically plausible upper
801 bound of sea-level rise projections, *Climatic Change*, 115, 893-902, 10.1007/s10584-012-
802 0610-6, 2012.
803 Stocker, T.: Model Hierarchy and Simplified Climate Models, in: *Introduction to Climate*
804 *Modelling, Advances in Geophysical and Environmental Mechanics and Mathematics*,
805 Springer Berlin Heidelberg, 25-51, 2011.
806 Takahashi, T., Sutherland, S. C., Wanninkhof, R., Sweeney, C., Feely, R. A., Chipman,
807 D. W., Hales, B., Friederich, G., Chavez, F., Sabine, C., Watson, A., Bakker, D. C. E.,
808 Schuster, U., Metzl, N., Yoshikawa-Inoue, H., Ishii, M., Midorikawa, T., Nojiri, Y.,
809 Körtzinger, A., Steinhoff, T., Hoppema, M., Olafsson, J., Arnarson, T. S., Tilbrook, B.,
810 Johannessen, T., Olsen, A., Bellerby, R., Wong, C. S., Delille, B., Bates, N. R., and de
811 Baar, H. J. W.: Climatological mean and decadal change in surface ocean pCO₂, and net
812 sea-air CO₂ flux over the global oceans, *Deep Sea Research Part II: Topical Studies in*
813 *Oceanography*, 56, 554-577, <http://dx.doi.org/10.1016/j.dsr2.2008.12.009>, 2009.
814 Tanaka, K., Kriegler, E., Bruckner, T., Hooss, C., Knorr, W., and Raddatz, T.:
815 Aggregated Carbon Cycle, Atmospheric Chemistry, and Climate Model (ACC2) -
816 description of the forward and inverse models, Max Planck Institute for Meteorology,
817 Hamburg, Germany, 188, 2007a.
818 Tanaka, K., Kriegler, E., Bruckner, T., Hooss, G., Knorr, W., Raddatz, T. J., and Tol, R.:
819 Aggregated carbon cycle, atmospheric chemistry, and climate model (ACC2), Hamburg,
820 188, 2007b.
821 Taylor, K. E., Stouffer, R. J., and Meehl, G. A.: An Overview of CMIP5 and the
822 Experiment Design, *Bulletin of the American Meteorological Society*, 93, 485-498,
823 10.1175/BAMS-D-11-00094.1, 2012.
824 Urban, N. M., and Keller, K.: Complementary observational constraints on climate
825 sensitivity, *Geophysical Research Letters*, 36, L04708, 10.1029/2008GL036457, 2009.
826 Urban, N. M., and Keller, K.: Probabilistic hindcasts and projections of the coupled
827 climate, carbon cycle and Atlantic meridional overturning circulation system: a Bayesian
828 fusion of century-scale observations with a simple model, *Tellus A*, 62, 737-750,
829 10.1111/j.1600-0870.2010.00471.x, 2010.
830 van Vuuren, D., Elzen, M. J., Lucas, P., Eickhout, B., Strengers, B., Ruijven, B., Wonink,
831 S., and Houdt, R.: Stabilizing greenhouse gas concentrations at low levels: an assessment

832 of reduction strategies and costs, *Climatic Change*, 81, 119-159, 10.1007/s10584-006-
833 9172-9, 2007.

834 van Vuuren, D., Lowe, J., Stehfest, E., Gohar, L., Hof, A., Hope, C., Warren, R.,
835 Meinshausen, M., and Plattner, G.-K.: How well do integrated assessment models
836 simulate climate change?, *Climatic Change*, 104, 255-285, 10.1007/s10584-009-9764-2,
837 2011.

838 Ward, D. S., and Mahowald, N. M.: Contributions of developed and developing countries
839 to global climate forcing and surface temperature change, *Environmental Research*
840 *Letters*, 9, 074008, 2014.

841 Wigley, T. M. L.: A simple inverse carbon cycle model, *Global Biogeochemical Cycles*,
842 5, 373-382, 10.1029/91GB02279, 1991.

843 Wigley, T. M. L.: Global-mean temperature and sea level consequences of greenhouse
844 gas concentration stabilization, *Geophysical Research Letters*, 22, 45-48,
845 10.1029/94GL01011, 1995.

846 Wigley, T. M. L., Richels, R., and Edmonds, J. A.: Economic and environmental choices
847 in the stabilization of atmospheric CO₂ concentrations, *Nature*, 379, 240-243, 1996.

848 Wigley, T. M. L., Smith, S. J., and Prather, M. J.: Radiative Forcing Due to Reactive Gas
849 Emissions, *Journal of Climate*, 15, 2690-2696, 10.1175/1520-
850 0442(2002)015<2690:RFDTRG>2.0.CO;2, 2002.

851 Wise, M., Calvin, K., Thomson, A., Clarke, L., Bond-Lamberty, B., Sands, R., Smith, S.
852 J., Janetos, A., and Edmonds, J.: Implications of Limiting CO₂ Concentrations for Land
853 Use and Energy, *Science*, 324, 1183-1186, 10.1126/science.1168475, 2009.

854 Wolkovich, E. M., Regetz, J., and O'Connor, M. I.: Advances in global change research
855 require open science by individual researchers, *Global Change Biology*, 18, 2102-2110,
856 10.1111/j.1365-2486.2012.02693.x, 2012.

857 Zeebe, R. E., and Wolf-Gladrow, D.: *CO₂ in Seawater: Equilibrium, Kinetics, Isotopes*,
858 Elsevier, 2001.

859

860

861 **Table and Figure Captions:**

862 **Table 1:** Initial model conditions prior to the spinup phase. Carbon values change
 863 slightly after spinning up to a steady state.

864

Variable	Description	Initial Value	Units	Notes
*C _{atm}	Atmospheric Carbon	588.1	PgC	Murakami(2010)
*C _D	Detritus Carbon	55.0	PgC	Denman et al., (2007) Land carbon (detritus, soil and vegetation) totaling ~2300PgC
*C _S	Soil Carbon	1782.0	PgC	
*C _V	Vegetation Carbon	550.0	PgC	
C _{DO}	Deep Ocean	26000.0	PgC	Denman et al., (2007) Ocean carbon (deep, intermediate and surface) totaling ~3800PgC **
C _{HL}	Surface Ocean High Latitude	140.0	PgC	
C _{IO}	Intermediate Ocean	8400.0	PgC	
C _{LL}	Surface Ocean Low Latitude	770.0	PgC	
F _L	Atmosphere-Land Carbon Flux	0.0	PgC yr ⁻¹	
F _O	Atmosphere-Ocean Carbon Flux	0.0	PgC yr ⁻¹	
NPP ₀	Net Primary Production	50.0	PgC yr ⁻¹	Approximate global value. Nemani et al., (2003)
T _G	Global Temperature Anomaly	0.0	°C	
T _{HL}	Temperature of high latitude surface ocean box	2.0	°C	Lenton, (2000)
T _{LL}	Temperature of low latitude surface ocean box	22.0	°C	Lenton, (2000)

865 * parameters appearing in the input file.

866 ** in order to obtain a steady state in Hector, carbon values in the intermediate box are

867 less than reported Denman et al.,(2007).

868 **Table 2:** Model parameters for the land and ocean carbon components.

Variable	Description	Value	Notes
f_{ds}	annual fraction of detritus carbon that is transferred to soil	0.60	The following fractions (f) were selected to be generally consistent with previous simple earth system models (e.g., Meinshausen et al., 2011a; Ricciuto et al., 2008; Murakami et al., 2010).
$*f_{ld}$	annual fraction of land use change flux from detritus	0.01	
f_{ls}	annual fraction of land use change flux from soil	0.89	
$*f_{lv}$	annual fraction of land use change flux from vegetation	0.10	
$*f_{nd}$	annual fraction of NPP carbon that is transferred to detritus	0.60	
f_{ns}	annual fraction of NPP carbon that is transferred to soil	0.05	
$*f_{nv}$	annual fraction of NPP carbon that is transferred to vegetation	0.35	
f_{rd}	annual fraction of respiration carbon that is transferred to detritus	0.25	
f_{rs}	annual fraction of respiration carbon that is transferred to soil	0.02	
f_{vd}	annual fraction of vegetation carbon that is transferred to detritus	0.034	
f_{vs}	annual fraction of vegetation carbon that is transferred to soil	0.001	
$*\beta$	Beta	0.36	
$*Q_{10}$	Q10 respiration	2.45	
$*T_H$	High-latitude circulation	$4.9e7 \text{ m}^3 \text{ s}^{-1}$	Tuned to give ~100 PgC from surface to deep
$*T_T$	Thermohaline circulation	$7.2e7 \text{ m}^3 \text{ s}^{-1}$	Tuned to give ~100

			PgC from surface to deep
*E _{ID}	Water mass exchange – intermediate to deep	1.25e7 m ³ s ⁻¹	Lenton, 2000; Knox and McElroy, 1984
*E _{LI}	Water mass exchange – low latitude to intermediate	2.0e8 m ³ s ⁻¹	Lenton, 2000; Knox and McElroy, 1984

869

870

* parameters appearing in the input file.

871 **Table 3:** CMIP5 ESM models used within this study. We use the same suite of models as
 872 found in Friedlingstein et al. (2014). Note, not all variables are reported for each model
 873 under all scenarios.
 874

Model	Model Name	Institute
bcc-csm1-1	Beijing Climate Center, Climate System Model, version 1.1	Beijing Climate Center, China Meteorological Administration, China
CanESM2 *	Second Generation Canadian Earth System Model	Canadian Center for Climate Modeling and Analysis, BC, Canada
CESM1-BGC *	Community Earth System Model, version 1.0-Biogeochemistry	National Center for Atmospheric Research, United States
GFDL-ESM2G	Geophysical Fluid Dynamic Laboratory Earth System Model with GOLD ocean component	Geophysical Fluid Dynamics Laboratory, United States
HadGEM2-ES	Hadley Centre Global Environmental Model, version 2 (Earth System)	Met Office Hadley Centre, United Kingdom
inmcm4	Institute of Numerical Mathematics Coupled Model, version 4.0	Institute of Numerical Mathematics, Russia
IPSL-CM5A-LR	L'Institut Pierre-Simon Laplace Coupled Model, version 5A, coupled with NEMO, low resolution	Institut Pierre Simon Laplace, France
MIROC-ESM *	Model for Interdisciplinary Research on Climate, Earth System Model	Atmosphere and Ocean Research Institute; National Institute for Environmental Studies, Japan Agency for Marine-Earth Science and Technology, Japan
MPI-ESM-LR	Max Planck Institute Earth System Model, low resolution	Max Planck Institute for Meteorology, Germany
MRI-ESM1 *	Meteorological Research Institute Earth System Model, version 1	Meteorological Research Institute Earth, Japan
NorESM1-ME *	Norwegian Earth System Model, version 1, intermediate	Norwegian Climate Center, Norway

resolution

* Models used in emissions forced scenarios (esmhist and esmrp85).

875 **Table 4:** Root mean square error (RMSE) for Hector versus observations, CMIP5, and
 876 MAGICC for atmospheric [CO₂], surface temperature anomaly, radiative forcing, fluxes
 877 of carbon (ocean and land), and low latitude surface ocean pH and change (Δ) in
 878 atmospheric [CO₂], surface temperature anomaly and radiative forcing for Hector,
 879 CMIP5, observations, and MAGICC6.

		Historical 1850 - 2005				
Variable		Hector	Observations	MAGICC	CMIP5	Units
[CO ₂]*	RMSE	--	2.85	2.95	2.21	ppmv
	Δ	85.78	94.47	95.0	103.30	
temperature	RMSE	--	0.15	0.13	0.15	deg C
	Δ	0.98	0.91	0.76	1.01	
Forcing	RMSE	--	--	0.39	--	W m ⁻²
	Δ	2.16	--	1.75	--	
Ocean Flux	RMSE	--	--	--	0.25	PgC yr ⁻¹
Land Flux	RMSE	--	--	--	1.27	PgC yr ⁻¹
pH	RMSE	--	--	--	0.004	unitless

*[CO₂] observations are an average of Law Dome and Mauna Loa.

		RCP 8.5 1850 - 2300				
Variable		Hector	MAGICC	CMIP5	Units	
[CO ₂] *	RMSE	--	10.41	7.54	ppmv	
	Δ	1557.91	1695.0	--		
temperature	RMSE	--	0.12	0.52	deg C	
	Δ	9.58	8.05	10.57		
Forcing	RMSE	--	0.26	--	W m ⁻²	
	Δ	12.80	12.24	--		
Ocean Flux	RMSE	--	--	1.39	PgC yr ⁻¹	
Land Flux	RMSE	--	--	3.86	PgC yr ⁻¹	
pH	RMSE	--	--	0.003	unitless	

*CMIP5 [CO₂] only to 2100.

880

RCP 8.5 2005 - 2300

Variable		Hector	MAGICC	CMIP5	Units
[CO ₂]*	RMSE	--	10.07	7.23	ppmv
	Δ	1472.13	1600.0	--	
temperature	RMSE	--	0.09	0.58	deg C
	Δ	8.59	7.30	9.57	
Forcing	RMSE	--	0.03	--	W m ⁻²
	Δ	10.65	10.49	--	
Ocean Flux	RMSE	--	--	1.41	PgC yr ⁻¹
Land Flux	RMSE	--	--	4.59	PgC yr ⁻¹
pH	RMSE	--	--	0.001	unitless

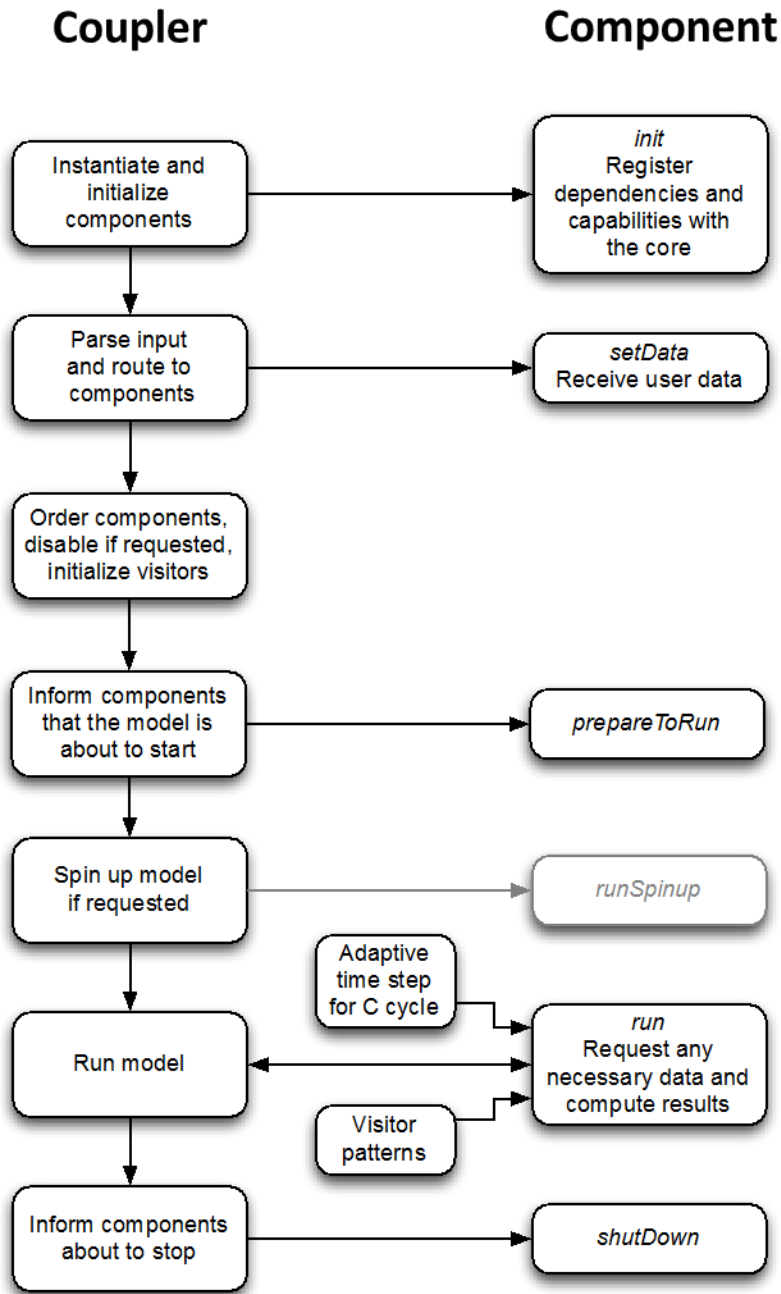
*CMIP5 [CO₂] only to 2100.

881

882

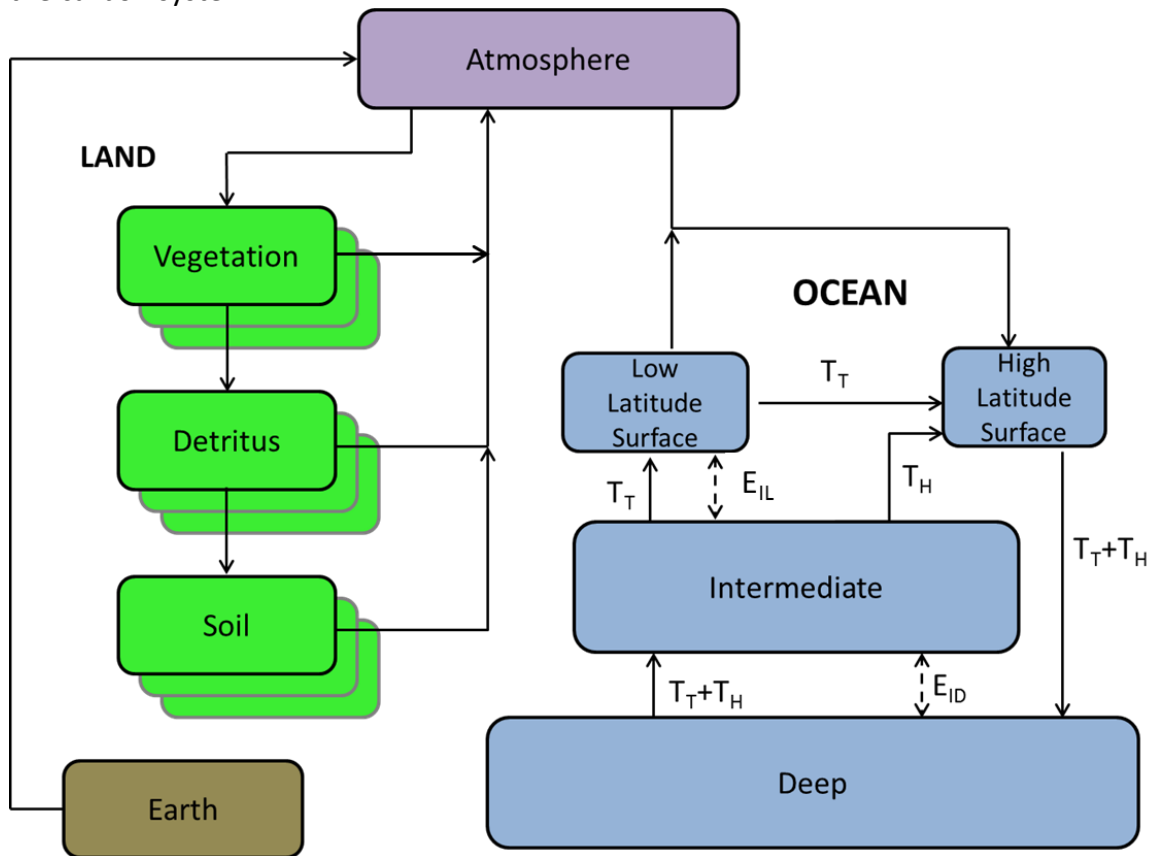
883

884 **Figure 1:** Model phases for the coupler (left) and a typical component (right). Arrows
 885 show flow of control and data. The greyed spinup step is optional.



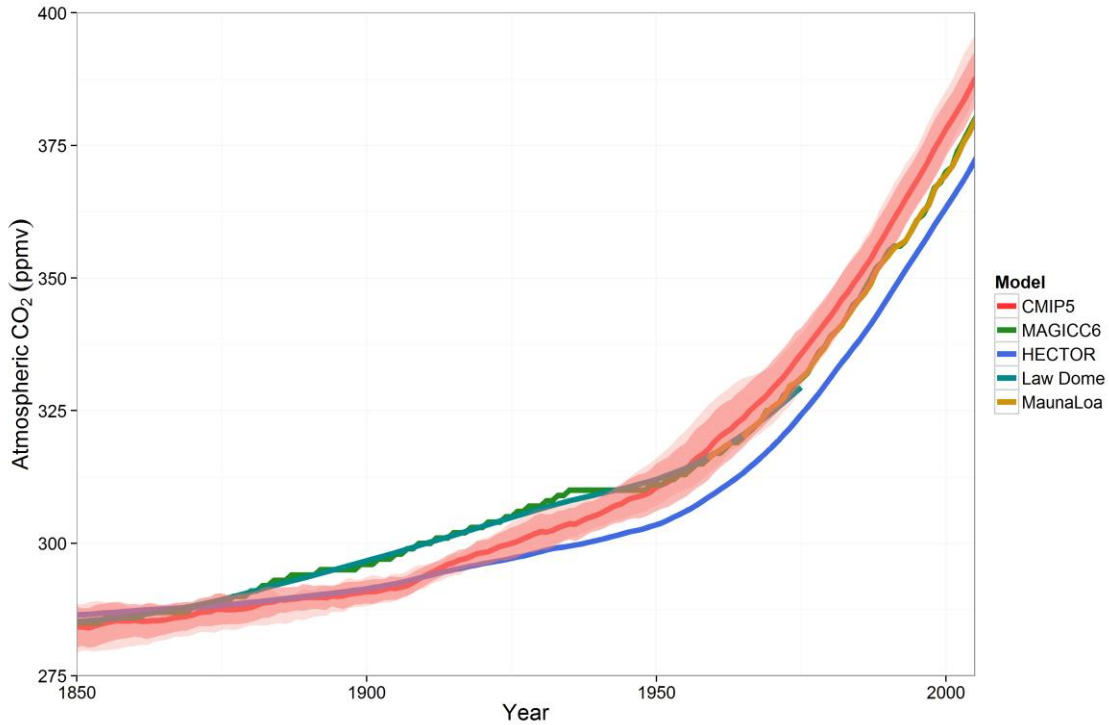
886
887

888 **Figure 2:** Representation of Hector’s carbon cycle, land, atmosphere, and ocean. The
 889 atmosphere consists of one well mixed box. The ocean consists of four boxes, with
 890 advection and water mass exchange simulating thermohaline circulation (see Table 2 for
 891 description of parameters). At steady state, the high latitude surface ocean takes up
 892 carbon from the atmosphere, while the low latitude surface ocean off gases carbon to
 893 the atmosphere. The land consists of a user defined number of biomes or regions for
 894 vegetation, detritus and soil. At steady state the vegetation takes up carbon from the
 895 atmosphere while the detritus and soil release carbon back into the atmosphere. The
 896 earth pool is continually debited with each time step to act as a mass balance check on
 897 the carbon system.



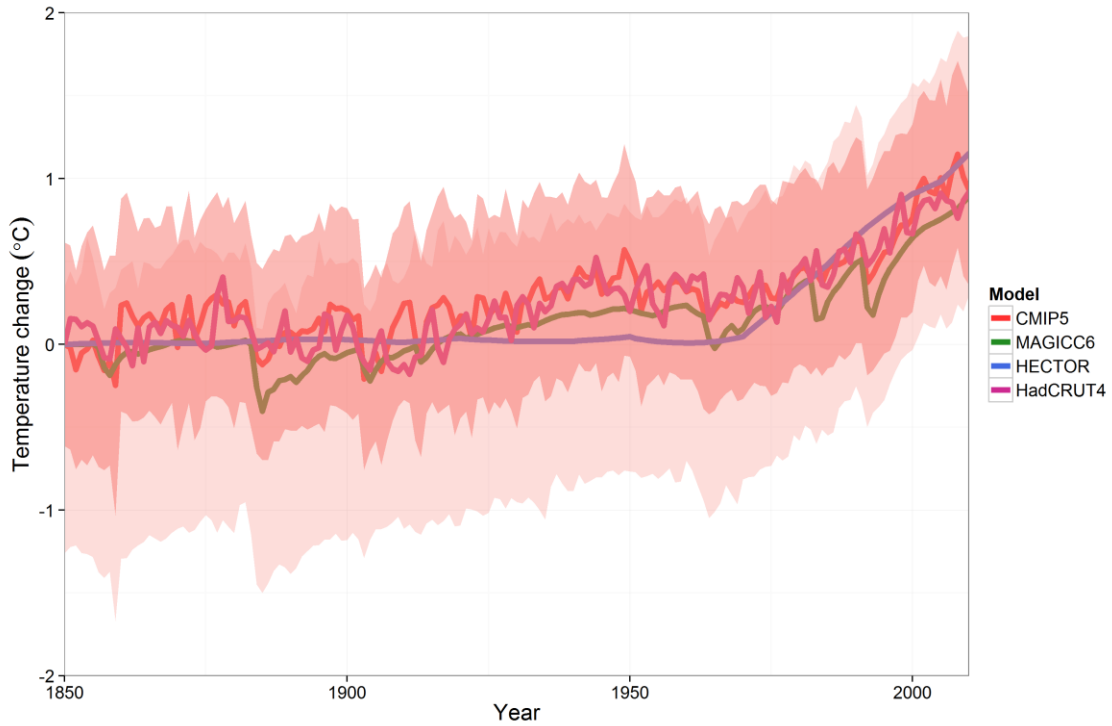
898
 899
 900

901 **Figure 3:** Historical atmospheric [CO₂] from 1850 to 2005 for Hector (blue), CMIP5
902 median, standard deviation, and model range (pink, n=4), MAGICC6 (green), Law Dome
903 (teal), and Mauna Loa (brown). Note CMIP5 data are from the prescribed emissions
904 historical scenario (esmHistorical). MAGICC6, however, is constrained to match the
905 observational record. Although Hector can be run with similar constraints, in this study
906 Hector was unconstrained to highlight the full performance of the model. n=4 is the
907 number of CMIP5 models used to produce this figure.



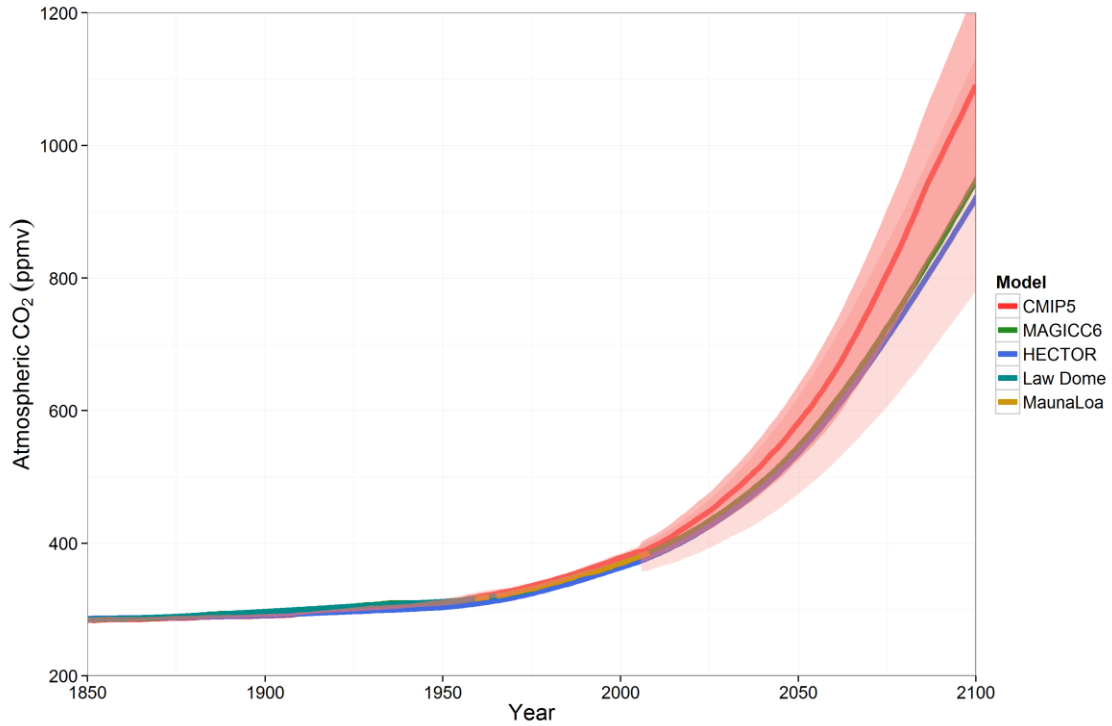
908
909
910

911 **Figure 4:** Historical global temperature anomaly relative to 1850 for Hector (blue),
912 MAGICC6 (green), CMIP5 median, standard deviation and model range (pink, n=8), and
913 historical observations from HadCRUT4 (purple). Hector is running without the effects of
914 volcanic forcing, leading to a smoother representation of temperature with time.
915



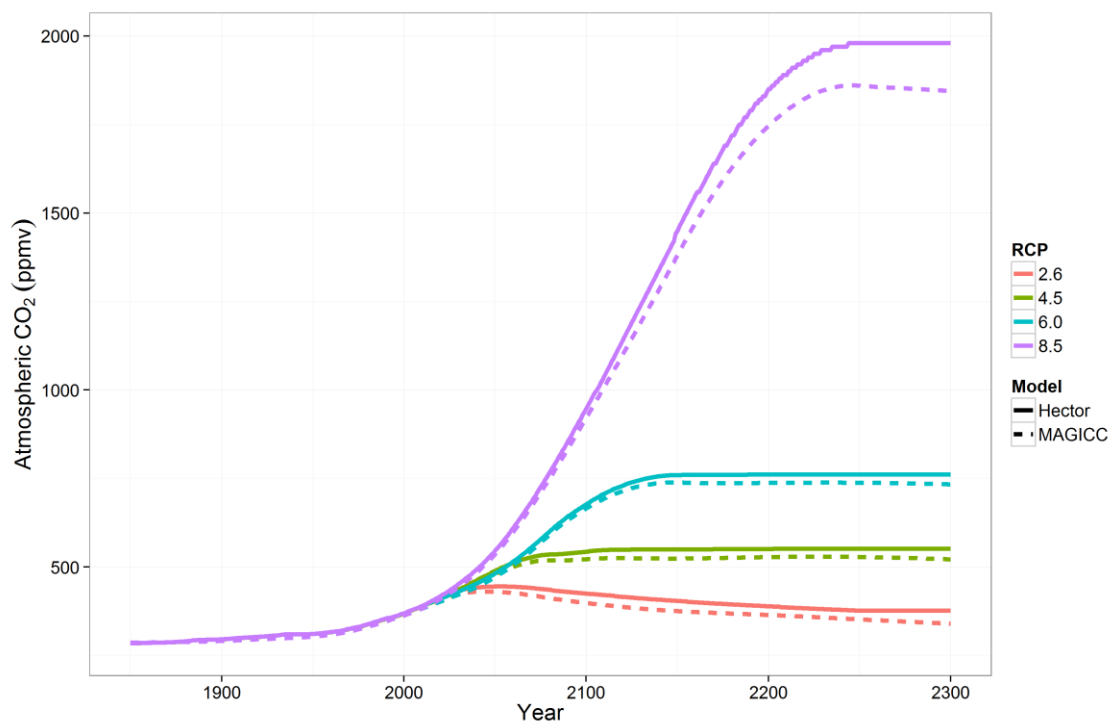
916

917 **Figure 5:** Atmospheric [CO₂] from 1850 to 2100 under RCP 8.5 for Hector (blue),
918 MAGICC6 (green), Mauna Loa (brown), Law Dome (teal) and esmRCP 8.5 (prescribed
919 emissions scenario) CMIP5 median, one standard deviation and model range (pink, n=4
920 (1850-2000) and n=5 (2001-2100)). Note that the CMIP5 models run under esmrcp85
921 do not extend to 2300.



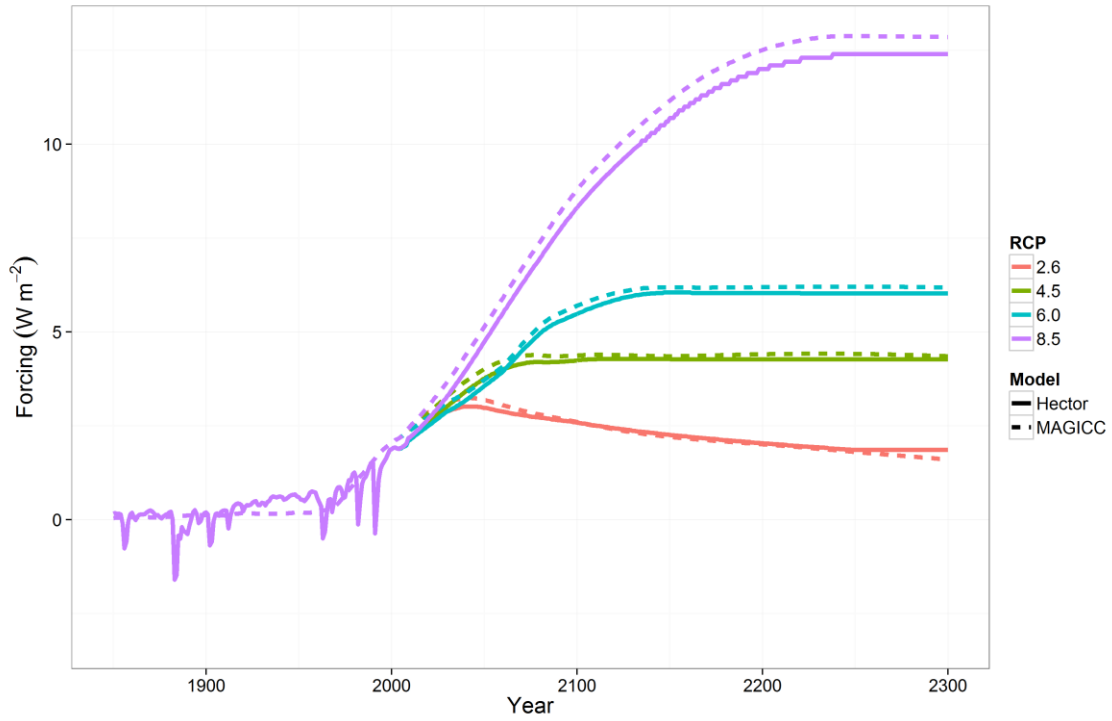
922
923

924 **Figure 6:** Atmospheric [CO₂] from 1850 to 2300 for RCP 2.6 (red), RCP 4.5 (green), RCP
925 6.0 (blue), RCP 8.5 (purple), Hector (solid) and MAGICC6 (dashed).
926



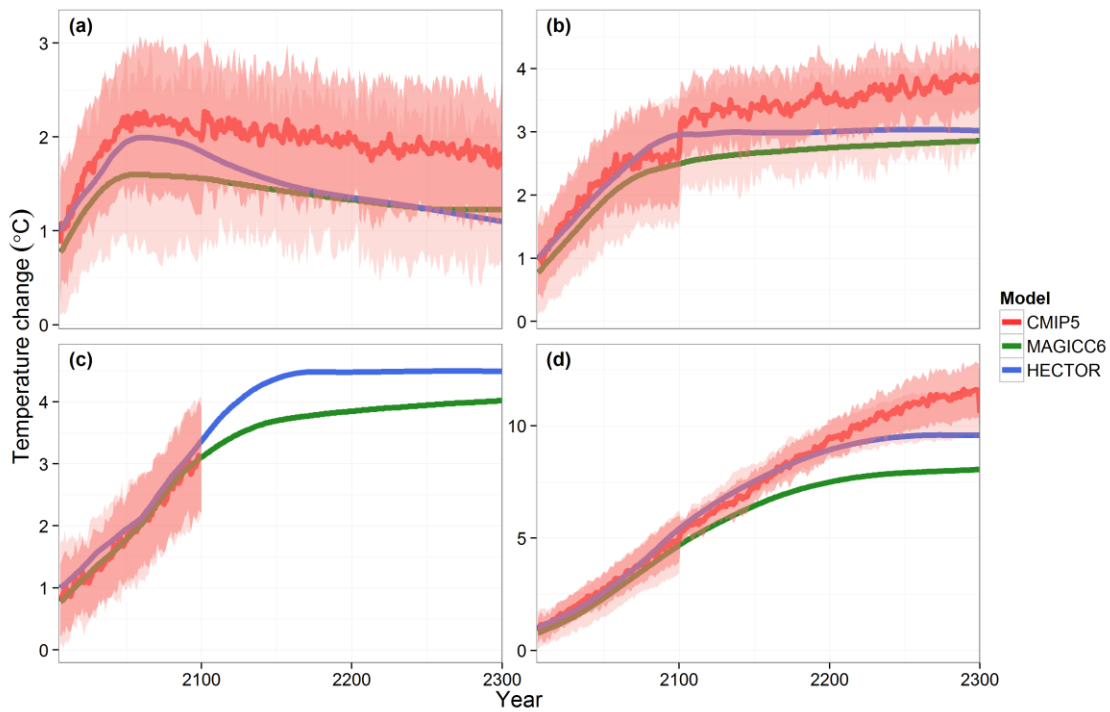
927
928

929 **Figure 7:** Relative radiative forcing from 1850 to 2300 for Hector (solid) and MAGICC6
930 (dashed) for all four RCP scenarios, 2.6 (red), 4.5 (green), 6.0 (blue), 8.5 (purple). Hector
931 has the option to enable or disable radiative forcing from historical volcanic emissions.
932 We have opted to disable this for ease of comparison across all RCPs.
933



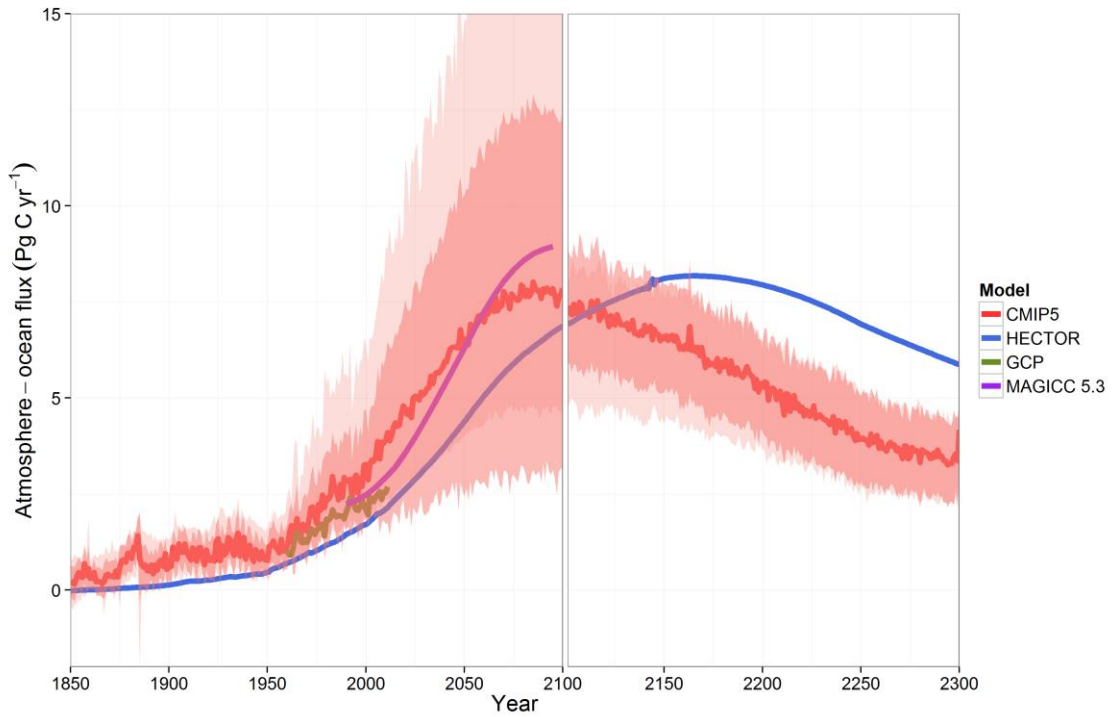
934
935

936 **Figure 8:** Global temperature anomaly relative to 1850 for (a) RCP 2.6 (b) RCP 4.5 (c) RCP
 937 6.0 and (d) RCP 8.5, comparing Hector (blue), MAGICC6 (green), and CMIP5 median,
 938 standard deviation and model range (pink). The CMIP5 models under RCP 6.0 used in
 939 this study do not extend to 2300. Note the change in scales between the four panels.
 940 Number of CMIP5 models in a) n=7 (2006-2100) and n=5 (2101-2300), b) n=9 (2006-
 941 2100) and n=6(2101-2300), c) n=6 (2006-2100), d) n=9 (2006-2100) and n=3 (2101-
 942 2300).



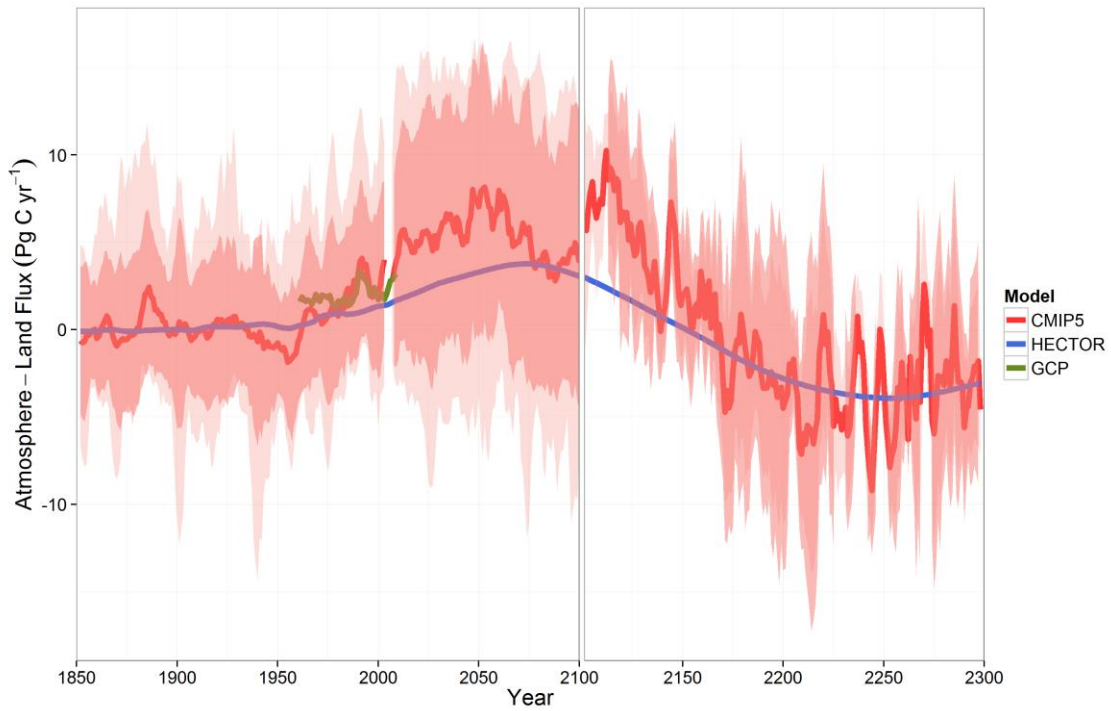
943
 944

945 **Figure 9:** Global air-sea fluxes of carbon under RCP 8.5, Hector (blue), MAGICC5.3
946 (purple, note that this is not the current version of MAGICC), CMIP5 median, standard
947 deviation, and model range (pink, n=9 (1850-2100) and n=4 (2101-2300)), and
948 observations from GCP (green) (Le Quéré et al., 2013). The break in the graph at 2100
949 signifies a change in the number of models that ran the RCP 8.5 extension.



950
951

952 **Figure 10:** Global air-land fluxes of carbon under RCP 8.5, Hector (blue), CMIP5 median,
953 standard deviation, and model range (pink, n=8 (1850-2100) and n=2 (2101-2300)), and
954 observations from GCP (green) (Le Quéré et al., 2013). The break in the graph at 2100
955 signifies a change in the number of models that ran the RCP 8.5 extension.
956



958 **Figure 11:** Low latitude (< 55) ocean pH for RCP 8.5, from 1850 – 2100, Hector (blue),
959 CMIP5 median, standard deviation, and model range (pink, n=6) and observations from
960 BATS (green) and HOTS (purple).
961

